# The 14th International Summer School on Advanced Studies of Polymer Electrolyte Fuel Cells

## Student Poster Session Abstracts

| No. | Name | Title |
|---|---|---|
| P1 | Fabio Blaschke | MANGANESE-IRON MIXED OXIDES AS OXYGEN CARRIER FOR CHEMICAL LOOPING HYDROGEN PRODUCTION |
| P2 | Hayato Enjoji | Parameter Determination of Start-Stop Simulated Accelerated Degradation Tests for Alkaline Water Electrolysis |
| P3 | Richard Hasso | DISPERSION BEHAVIOR OF GRAPHENE-BASED CATALYSTS |
| P4 | Mathias Heidinger | DERIVATE PHOTOMETRY AS A METHOD FOR THE DETERMINATION OF FLUORINE EMISSION RATES IN POLYMER ELECTROLYTE FUEL CELLS |
| P5 | Taiki Ishida | Effect of pore size and thickness of porous transport layers on the polarization of PEM water electrolysis |
| P6 | Daiki Kudo | THE EFFECT OF HYDROPHILIC CONTROL OF THE CATHODE FOR TOLUENE DIRECT-HYDROGENATION ELECTROLYZER |
| P7 | Kazuyuki Matsukawa | Performance Evaluation and Analysis of Bubble Detachment Factors for Alkaline Water Electrolyzer |
| P8 | Abdelhakim Merdjani | FRACTAL DESIGN OF FLOW FIELD PLATE FOR PEMFC |
| P9 | Daiji Mizukoshi | FORMATION OF METAL HYDROXIDE-BASED COMPOSITE ANODE CATALYSTS FOR ALKALINE WATER ELECTROLYSIS VIA CO-ELECTRODEPOSITION OF HYBRID COBALT HYDROXIDE NANOSHEETS |
| P10 | Shota Oi | Relationship between Faraday efficiency and drag water for electrochemical toluene hydrogenation |
| P11 | Nikhat Pasha | Polyaniline coating of carbon to increase corrosion resistance |
| P12 | Michaela Roschger | HALF-CELL MEASUREMENTS OF PALLADIUM-BASED CATALYSTS FOR ETHANOL OXIDATION |
| P13 | Taiki Sano | ENHANCED H2 BUBBLE REMOVAL FROM CATHODE OF ALKALINE WATER ELECTROLYZER BY COATING WITH HYDROPHILIC HYBRID MAGNESIUM HYDROXIDE NANOSHEET |
| P14 | Kohei Serizawa | PREPARATION OF NANOPARTICURATE CATALYSTS FOR POLYMER ELECTROLYTE FUEL CELL CATHODE USING ZR-BASED CLUSTER AS PRECURSOR |
| P15 | Dmytro Stepanov | Investigation of the Cycling Stability of Room-Temperature Metal Hydrides (MHs) |
| P16 | Bernd Stoppacher | UTILIZATION OF RAW BIOGAS FOR HIGH-PURITY HYDROGEN PRODUCTION VIA CHEMICAL LOOPING |
| P17 | Fumiyasu Suito | Performance Analysis of Protonic Ceramic Fuel Cell Cogeneration System<br>using Methane Fuel |
| P18 | Daichi Suzuki | EFFECTS OF SURFACE TEXTURE FOR VAPOR CONDENSATION WITH NON-CONDENSABLE GAS |
| P19 | Ryogo Takatera | NUMERICAL ANALYSIS OF DEPENDENCE OF LEAKAGE CURRENT ON GAS PARTIAL PRESSURES IN PCFC |

| No. | Name | Title |
|---|---|---|
| P20 | Yu Takenaga | NUMERICAL ANALYSIS OF DEPENDENCE OF LEAKAGE CURRENT ON GAS PARTIAL PRESSURES IN PCFC |
| P21 | Florian Tritscher | COATINGS FOR ADVANCED FUNCTIONALIZED GAS DIFFUSION LAYERS IN FUEL CELLS |
| P22 | Kohei Wakuda | INVESTIGATION OF DISSOLVED OXYGEN FIELD BY VISUALIZING OXYGEN BUBBLES NEAR ANODE CATALYST ELECTRODE IN PEM WATER ELECTROLYZER |
| P23 | Sigrid Wolf | CARBON-SUPPORTED SILVER/MANGANESE OXYDE CATALYSTS FOR THE OXYGEN REDUCTION REACTION IN ALKALINE MEDIA |
| P24 | Ritsuki Nakajima | PREPARATION AND EVALUATION OF HYDROGEL ELECTRODES WITH HIGH RELEASING ABILITY OF EVOLVED BUBBLES |
| P25 | Sunpil Jang | VISUALIZATION OF HYDROGEN BUBBLES IN POROUS TRANSPORT LAYER IN TOLUENE DIRECT-ELECTRO-HYDROGNATION ELECTROLYZER USINIG X-RAY-CT SYSTEM |

# MANGANESE-IRON MIXED OXIDES AS OXYGEN CARRIER FOR CHEMICAL LOOPING HYDROGEN PRODUCTION

Fabio Blaschke[1], and Viktor Hacker[1]

[1] Working Group Fuel Cells and Hydrogen, Institute of Chemical Engineering and Environmental Technology Graz University of Technology, Inffeldgasse 25/C/EG, 8010 Graz, Austria, blaschke@tugraz.at

**Keywords:** Hydrogen Production, Chemical Looping, Oxygen Carrier and Manganese Iron Oxide

## INTRODUCTION

More than 99 % of the produced hydrogen for industrial application is still derived from fossil fuels. Due to global warming, new technologies for the production of green hydrogen need to be developed. The chemical looping technology is a promising technique for the production of green and high-pressurized hydrogen from syngas by using steam as oxidant [1]. Nevertheless the bottleneck of this process is the availability of highly stable oxygen carrier pellets in fixed bed process [2].Many different support materials in combination with iron have already been tested. Especially, perovskite material demonstrated good performance due to the change in chemical properties of the iron. Iron with manganese is a promising combination because of its low cost, non-toxicity and good thermal stability during the chemical-looping process. Moreover, DFT calculations and experimental results have shown potentially high conversion of syngas in chemical looping combustion processes in small scale [3,4,5].

The aim of this work was to investigate the usability of the combination of manganese-iron oxide oxygen carrier (OC) for the production of hydrogen in large scale with a good cyclic stability. Additional the material synthesis should be environmental friendly and cost efficient, without using any additional inert support material to have a high specific hydrogen production (SHP).

A manganese-iron oxygen carrier was synthesised with two different synthesis techniques. This was done with a solid solution method by using metal oxides and a sol-gel method by using nitrates as starting materials. The stoichiometric ratio was set to Mn:Fe = 1:2 mol. The reduction and oxidation performance of the two different synthesis routes was investigated in the form of powders in a 40 mg scale with thermogravimetric analysis. The results show that a constant reduction and oxidation performance was achieved for both synthesis methods. Additional a time programmed reduction analysis before and after the cyclisation was performed to detect changes in the reactivity. No significant differences in the reduction performance were found between the nitrates or metal oxides synthesized OCs. Based on the results, a long cyclic study with 40 cycles was performed for each material. The less expensive and environmentally friendly solid solution method showed the same reduction and oxidation performance over a larger number of cycles (Fig. 1 a.). Scanning electron microscopy showed the formation of a sponge-like morphology, which explains the good cycling stability by suppressing sintering phenomena (Fig. 1 b.). The morphology also explains the fast release of hydrogen during the oxidation step due to the micro holes in the structure. The solid solution synthesis route was scaled up to test the performance in a fixed bed system. Pellets were formed using distilled water as an additive in an intensive mixer. The OC carrier was calcined at 900 °C for 6 h. Stable pellets with a size of 2-4 mm were obtained after sieving. The prepared materials were tested in a 4 kW reactor with a sample amount of 250 g for 12 cycles. The results show that a combination of $Fe_2O_3$ and MnO without any support material is cycle stable and has a high hydrogen production value with a SHP above 10 $molH_2/kgOC$ per cycle (Fig. 2). The pellets in the reductive state did not show sintering behavior in the reactor after cyclisation, which is connected to the sponge like structure detected with SEM. Overall, with the solid solution an oxygen carrier that efficiently stores hydrogen, can be produced on a larger scale with an environmentally friendly and inexpensive material, and does not require any support material.

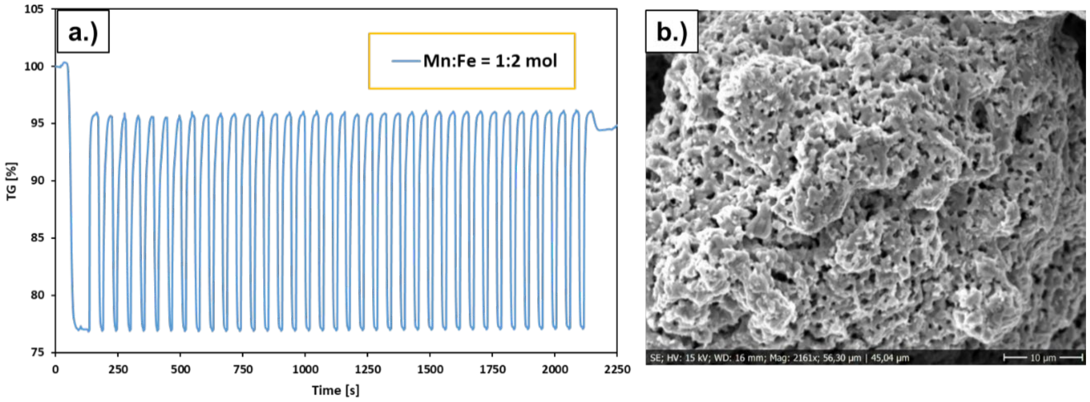

**Figure. 1** a.) Cyclisation of the OC synthesized in solid solution at a stoichiometric concentration of 1:2 mol Mn:Fe for 40 cycles. Each cycle was performed at 50 $mLH_2$/min for reduction and 2.44 g $H_2O$/h for oxidation for 30 min. b.) SEM picture of the OC after 40 Cycles in the reduced state.

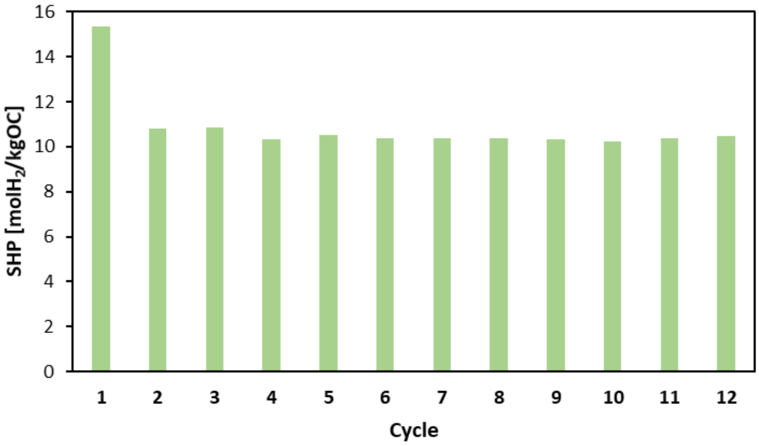

**Figure. 2** Specific hydrogen production (SHP) performance of 250g of manganese-ferrite OC synthesized in solid solution in a fixed-bed reactor cycle experiment.

## Acknowledgement

Financial support by the Austrian Science Fund (FWF): P 34824 is gratefully acknowledged.

## REFERENCES

[1] R. Zacharias, S. Visentin, S. Bock, and V. Hacker, “High-pressure hydrogen production with inherent sequestration of a pure carbon dioxide stream via fixed bed chemical looping,” Int. J. Hydrogen Energy, vol. 44, no. 16, pp. 7943–7957, Mar. 2019, doi: 10.1016/j.ijhydene.2019.01.257.

[2] R. Zacharias, S. Bock, and V. Hacker, “The impact of manufacturing methods on the performance of pelletized, iron-based oxygen carriers for fixed bed chemical looping hydrogen in long term operation,” Fuel Process. Technol., vol. 208, no. March, p. 106487, Nov. 2020, doi: 10.1016/j.fuproc.2020.106487.

[3] F. Liu, J. Liu, Y. Yang, and X. Wang, “A mechanistic study of CO oxidation over spinel MnFe2O4 surface during chemical-looping combustion,” Fuel, vol. 230, no. May, pp. 410–417, 2018, doi: 10.1016/j.fuel.2018.05.079.

[4] G. Azimi, T. Mattisson, H. Leion, M. Rydén, and A. Lyngfelt, “Comprehensive study of Mn-Fe-Al oxygen-carriers for chemical-looping with oxygen uncoupling (CLOU),” Int. J. Greenh. Gas Control, vol. 34, pp. 12–24, 2015, doi: 10.1016/j.ijggc.2014.12.022.

[5] H. Zhou et al., “Reaction performance and lattice oxygen migration of MnFe2O4 oxygen carrier in methane-carbon dioxide reaction system,” Int. J. Hydrogen Energy, vol. 45, no. 55, pp. 30254–30266, 2020, doi: 10.1016/j.ijhydene.2020.08.103.

P2

# Parameter Determination of Start-Stop Simulated Accelerated Degradation Tests for Alkaline Water Electrolysis

Hayato Enjoji[1], Ashraf Abdel Haleem[2], Kensaku Nagasawa[2], Yoshiyuki Kuroda[1,2] and Shigenori Mitsushima[1,2]
[1]*Graduate School of Engineering Science, Yokohama National University, 79-5 Tokiwadai, Hodogaya-ku, Yokohama 240-8501, Japan*
[2]*Institute of Advanced Sciences, Yokohama National University, 79-5 Tokiwadai, Hodogaya-ku, Yokohama 240-8501, Japan*
*cel@ml.ynu.ac.jp*

**Keywords:**. Alkaline Water Electrolysis, Reverse Current, Ni based Electrode, Accelerated Durability Test

## Introduction

Power to Gas (P2G) technology is expected to allow installation of a lot of renewable electricity without imbalance issue of electric power grid. Here, water electrolysis is a key device in the P2G. One of the conventional processes in water electrolysis is alkaline water electrolysis (AWE), which has the advantages of a low material cost. On the other hand, there is an issue of electrode degradation caused by the reverse current generated with frequent start-stop of renewable energy power source. Furthermore, detailed mechanism of electrode degradation under start-stop conditions has not been revealed. Therefore, it is necessary to establish simplified experimental method that can evaluate degradation by simulating start-stop conditions to develop a new durable electrode.

In this study, parameters for Accelerated Degradation Test (ADT) that simulated start, reverse current, and stop flows were determined using NiCo spinel catalyst coated Ni anode.

## Experimental

ADT was performed in a three-electrode cell with 7 M KOH aqueous as electrolyte at 25℃. RHE, Ni coil and 1 $cm^2$ Ni mesh electrode coated NiCo oxide catalyst are used as reference, counter and working electrodes, respectively. Constant current electrolysis at 1 $A/cm^2$ for 2 hours was conducted as pretreatment at 80℃ before ADT.

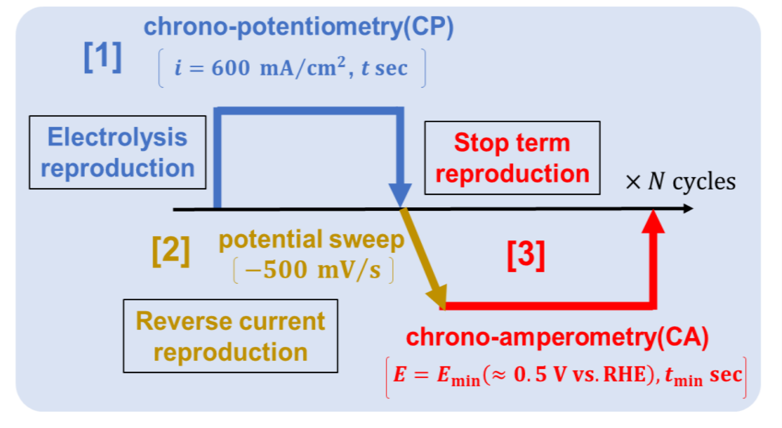

**Fig.1 Practical condition simulated ADT protocol outline drawing**

The ADT protocol consisted of three steps: (1) constant current electrolysis at 600 mA $cm^{-2}$ for 60 s simulated electrolysis operation, (2) potential scanning from OCP to anodic minimum potential : $E_{\mathrm{min}}$(=0.3, 0.5, 0.7, 1.3 V vs. RHE) at scanning rate of -500 mV/s as reverse current simulating, and (3) holding at constant potential of $E_{\mathrm{min}}$ for $t_{\mathrm{min}}$ (=10, 18, 30, 45, 60, 120 s) simulated stop operation as shown in Figure 1. [1]

To evaluate the oxygen evolution activity, Cyclic Voltammetry: CV (potential range: 0.5-1.8 V, scanning speed: 5, 50 mV/s, 3 cycles) and AC impedance measurements (bias potential: 1.6 V, frequency range: $10^6$-$10^{-1}$ Hz, amplitude: 10 mV) were performed basically at every 200 ADT cycles in 2,000 cycles of ADT.

## Results & Discussions

Figure 2 shows (a) oxygen evolution reaction currents of CV (v = 5 mv/s) and (b) anode potential at $i$ = 50 $mA/cm^2$ of the CVs as function of ADT cycles for each $E_{\mathrm{min}}$. Under the $E_{\mathrm{min}}$ = 0.3~0.7 V condition, the potential increase to about 1.8 V was observed around 2,000 cycles of

ADT, but under the $E_{\min}$ = 1.3 V condition, no potential increase was observed and the behavior was the same as no start-stop electrolysis. This difference is due to redox of Co and Ni around 1.2 V vs. RHE.[2,3] and repeated redox cycles of the catalyst caused by potential fluctuations from start-stop would lead the degradation.

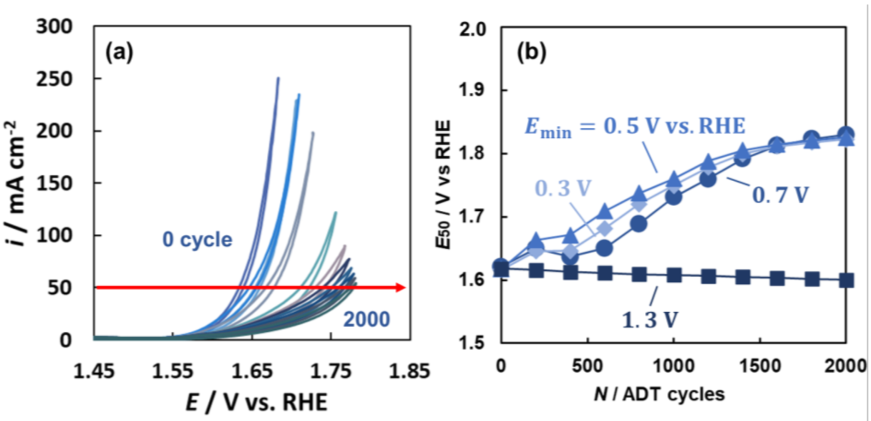

Fig.2 (a) Cyclic voltammetry at $E_{\min} = 0.5$ V vs. RHE conditions ($v = 5$ mV/s) (b) Cycle dependence of anode potential at $i = 50$ mA/cm$^2$ of the CV

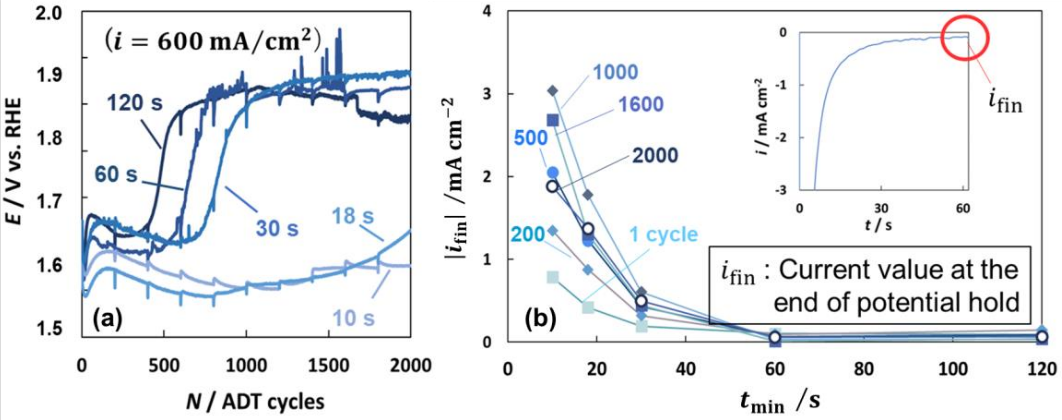

Fig.3 (a) Potential at 600 mA/cm$^2$ as a function of ADT cycle number with 10 to 120 s of $t_{\min}$ at 0.5 V vs. RHE and (b) The relationship between $i_{\mathrm{fin}}$ and $t_{\min}$ at that time

Figure 3 (a) shows the anode potential at $i$ =600 mA/cm$^2$ at $t_{\min}$ =10~120 s under $t_{\min}$ =0.5 V where catalyst redox occurs. For the longer $t_{\min}$, the earlier potential increase was observed. This indicates that the degradation acceleration per cycle is greater with longer $t_{\min}$ is longer. Figure 3 (b) shows the relationship between $t_{\min}$ and $i_{\mathrm{fin}}$ (current at the end of $E_{\min}$ hold). It can be seen that $i_{\mathrm{fin}}$ converges to around 0 at about $t_{\min}$ =60 s. Therefore, it is assumed that Ni and Co, which changed valence during potential sweeping, are eluted during the potential holds.

In conclusion, in the case of ADT using Ni or Co catalysts, it is essential to set the holding potential for stop reproduction at around 0.5V, well below the reduction potential. In addition, the potential holding time of about 60 s is necessary to elute the catalyst components, and $t_{\min}$ =60 s was determined to be optimal from the perspective of shortening the ADT time in this study.

## Acknowledgements

This study was based on results obtained from the Development of Fundamental Technology for Advancement of Water Electrolysis Hydrogen Production in Advancement of Hydrogen Technologies and Utilization Project (JPNP14021) commissioned by the New Energy and Industrial Technology Development Organization (NEDO).

## References

[1] A. Abdel Haleem, K. Nagasawa, Y. Kuroda, Y. Nishiki, A. Zaenal, S. Mitsushima, Electrochemistry, 89(2), 186-191 (2021).

[2] Z. Liu, G. Wang, X. Zhu, Y. Wang, Y. Zou, S. Zang, S. Wang, Angew. Chem. Int. Ed. 59, 2-9 (2020).

[3] S. R. Mellsop, A. Gardiner, B. Johannessen, A. T. Marshall, Electrochimica Acta, 168, 356-364 (2015).

P3

# DISPERSION BEHAVIOR OF GRAPHENE-BASED CATALYSTS

HASSO Richard[1], ROSCHGER Michaela[1], WOLF Sigrid[1], GENORIO Boštjan[2], and HACKER Viktor[1]

[1] TU Graz, Institute of Chemical Engineering and Environmental Technology, Inffeldgasse 25/C, 8010 Graz, Austria, richard.hasso@tugraz.at
[2] University of Ljubljana, Faculty of Chemistry and Chemical Technology, Vecna pot 113, 1000 Ljubljana, Slovenia

**Keywords:** graphene-based catalysts, graphene dispersions

As a key component, the catalyst plays an important role in the performance of fuel cells (FCs). Since most catalysts used in FCs are usually of precious nature and therefore expensive, application methods must be efficient and material saving. As a result of this, the choice of support material and composition of the catalyst is crucial. Most prominent support materials currently used are carbon blacks, such as Vulcan, which show good electrical characteristics in combination with a large surface area and small achievable support-particle sizes [1]. Nevertheless, graphene gained a lot of attention within the last decade due to it`s also very promising characteristics. Although being the simplest form of carbon, it shows outstanding electron mobility and mechanical strength. Combined with even higher theoretical specific surface area compared to carbon blacks, the promising role of graphene-based support materials cannot be neglected [2]. Examples for graphene-based materials are graphene oxide (GO), reduced graphene oxide (rGO) and nitrogen doped reduced graphene oxide (NrGO) and can be seen in Fig. 1.

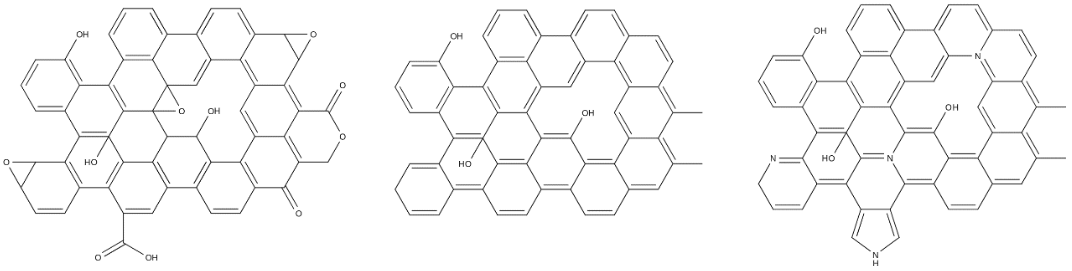

*Figure 1: Schematic structure of graphene-based support materials. From left to right: graphene oxide (GO), reduced graphene oxide (rGO) and N-doped reduced graphene oxide (NrGO).*

For application of the catalyst, usually, a catalyst containing dispersion (ink) is used. Depending on the method of application (e.g., spray coating), the composition of the ink and choice of the solvents are important, especially concerning the stability of the dispersion. Otherwise, separation or agglomeration of the particles may occur, resulting in inhomogeneous and inefficient catalyst layers [3]. A block diagram of the general catalyst ink preparation can be seen in Fig. 2.

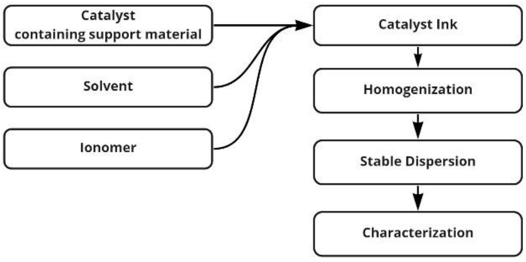

*Figure 2: Block diagram for the ink preparation.*

Outlook of this study is to test and analyze different ink compositions on their ability to form stable dispersions. For further information of obtained particle sizes in the dispersion, the zeta potential will be determined by dynamic light scattering.

## ACKNOWLEDGEMENT

The authors acknowledge the financial support by the Austrian Science Fund FWF I 3871-N37.

## REFERENCES

[1] K. Wikander et al., “Alternative Catalysts and Carbon Support Material for PEMFC”, Fuel Cells, no. 6, pp. 21 – 25 (2006)

[2] M. Liu, R. Zhang and W. Chen, “Graphene-Supported Nanoelectrocatalysts for Fuel Cells: Synthesis, Properties, and Applications”, Chemical Reviews 114 (10), pp. 5117–5160 (2014)

[3] M. Xie, T. Chu, T. Wang, K. Wan, D. Yang, B. Li, P. Ming, C. Zhang, “Preparation, Perfomance and Challenges of Catalyst Layer for Proton Exchange Membrane Fuel Cell”, Membranes, 11(11), p. 879 (2021)

# DERIVATE PHOTOMETRY AS A METHOD FOR THE DETERMINATION OF FLUORINE EMISSION RATES IN POLYMER ELECTROLYTE FUEL CELLS

Mathias Heidinger[1], Kurt Mayer [1], Joel Edjokola[1], Merit Bodner[1], Daniel Sandu[2], Hacker Viktor[1]

*[1]Graz University of Technology, Institute of Chemical Engineering and Environmental Technologies, Inffeldgasse 25C, 8010 Graz, Austria, mathias.heidinger@tugraz.at*
*[2]AiDEXA GmbH, Bergmanngasse 25 T10, 8010 Graz, Austria*

Degradation in polymer electrolyte fuel cells (PEFC) can be divided into chemical and physical degradation. Chemical degradation is greatly contributing to membrane degradation, which is a major contributor to reduced performance and lower efficiency. Chemical degradation of the membrane can be measured during operation, by analysing the effluent water from the cell. The chemical degradation is promoted by radical formation, which can occur on both the anode and the cathode side [1–3]. Low pH values and low relative humidities also increase chemical degradation by accelerating hydrogen peroxide ($H_2O_2$) production [4] and OCV conditions [5,6]. Oxygen-derived free radicals (HO* and HOO*) are formed in situ from hydrogen peroxide. These free radicals can react with the Nafion® membrane, leading to the emission of fluorides with the fuel cell exhaust. Fluoride emission and chemical degradation can also be caused by impurities in reactant gases or other sources of chemical degradation of the membrane [7,8]. Radical formation is enabled by Fenton active metals, whose presence can enable a homolytic oxygen bond cleavage, leading to radical formation [4]. Chemical degradation of the membrane can be identified by tracking the amount of fluorides in fuel cell effluent water.

Standards and synthetic test samples were prepared from ultrapure water and standard solutions. The fluoride concentration was determined using a calibration curve and standard addition. Potential interferences were evaluated by preparing test solutions, introducing different ions to standard samples. Matrix effects were evaluated by varying sample conditions to ensure consistent results. All samples are mixed with Zr(IV)-SPADNS2 and transferred to a cuvette for measurements [9].

Effluent water samples, standard and test samples are analysed using a UV-vis spectrometer developed by AiDEXA GmbH. This is done by monitoring the intensity in a given frequency range. The Zr(IV)-SPADNS2 will react with fluorine present in the samples, causing a quenching reaction that reduces intensity in the peak intensity as well as causing a shift to lower wavelengths. Results from measurements can then be correlated to electrochemical measurements to obtain information about the correlation between chemical membrane degradation and fluoride emission. With this correlation, external measurements could be used for lifetime estimation based on the fluoride concentration present in effluent fuel cell water.

## ACKNOWLEDGEMENT

This research is performed under the projects HyLife (K-Project HyTechonomy, FFG grant number 882510) and B.GASUS (FFG grant number 884368), which are supported by the Austrian Research Promotion Agency (FFG).

## REFERENCES

[1] P. Frühwirt, A. Kregar, J.T. Törring, T. Katrašnik, G. Gescheidt, Phys. Chem. Chem. Phys. 22 (2020) 5647–5666.
[2] A. Kregar, G. Tavčar, A. Kravos, T. Katrašnik, Appl. Energy 263 (2020) 114547.
[3] M. Bodner, A. Schenk, D. Salaberger, M. Rami, C. Hochenauer, V. Hacker, Fuel Cells 17 (2017) 18–26.
[4] M. Bodner, J. Senn, V. Hacker, in: Fuel Cells Hydrog. From Fundam. to Appl. Res., Elsevier, 2018, pp. 139–154.
[5] M. Bodner, C. Hochenauer, V. Hacker, J. Power Sources 295 (2015) 336–348.
[6] M. Bodner, B. Cermenek, M. Rami, V. Hacker, Membr. 2015, Vol. 5, Pages 888-902 5 (2015) 888–902.
[7] B. Shabani, M. Hafttananian, S. Khamani, A. Ramiar, A.A. Ranjbar, J. Power Sources 427 (2019) 21–48.
[8] X. Cheng, Z. Shi, N. Glass, L. Zhang, J. Zhang, D. Song, Z.S. Liu, H. Wang, J. Shen, J. Power Sources 165 (2007) 739–756.
[9] R.M. Patel, K.S. Patel, M.L. Naik, Int. J. Environ. Stud. 56 (1999) 745–756.

P5

# Effect of pore size and thickness of porous transport layers on the polarization of PEM water electrolysis

Taiki Ishida[1], Kensaku Nagasawa[2], Yoshiyuki Kuroda[1,2], Shigenori Mitsushima[1,2]

[1]Graduate school of Engineering Science, Yokohama National University, 79-5 Tokiwadai, Hodogaya-ku, Yokohama 240-8501, Japan, email: cel@ml.ynu.ac.jp
[2]Institute of Advanced Sciences, Yokohama National University, 79-5 Tokiwadai, Hodogaya-ku, Yokohama 240-8501, Japan: cel@ml.ynu.ac.jp

**Keywords:**. PEM water electrolysis, Porous transport layer, mass transfer, electron transfer

## Introduction

Renewable energies have been expected to be introduced to reduce $CO_2$ emission. However, to solve the imbalance between their variability, it is important to establish Power to Gas (P2G) technologies, which convert to hydrogen for storage and utilization. Proton exchange membrane water electrolysis (PEMWE) is one of the important P2G technologies and can operate in high current density region, but improvements are still required to reduce cost due to the stack cost like bipolar plates, noble metals, membrane and so on. Therefore, it is necessary to achieve high current density while maintaining efficiency for reduction of the system cost. The porous transport layer (PTL), which has roles such as supplying water to catalyst layer (CL), discharging the generated gas, and transporting electrons between the CL and bipolar or end plates, is an essential element in PEMWE[1]. Especially, PTLs morphology (ex. structure, pore size, porosity, thickness) has great impact on PEMWE performance in terms of mass transfer and electron transfer. In that case, the accurate separation of polarization into anode and cathode and evaluation of the effect of anode PTLs parameters on mass transfer and electron transfer are required.

In this study, we have investigated the effects of pore size and thickness of the anode PTLs on electrolysis performance to improve mass transfer and electron transfer in anode PTLs.

## Experimental

Anode and cathode electrocatalysts were $IrO_x$ (TKK, ELC-0110, 1.0 $mg_{Ir}/cm^2$) and Pt/C (TKK, TEC10E50E, 1.0 $mg_{Pt}/cm^2$), respectively. PEM was Nafion®115 (DuPont). Figure 1 shows the schematic drawing of 1 $cm^2$ electrolyzer. PTL itself or parallel were used on anode flow channel. Also, PTL itself was used on cathode flow channel. Platinum coated titanium (Mitsubishi Materials Corporation, Table.1) and the carbon paper (39BC, SIGRACET®GDL) were used as the anode and cathode PTLs, respectively. $H_2$ storage Pd references were placed on the membrane by the contact with 0.5 M $H_2SO_4$. Operation temperature of the electrolyzer conducted at 80 °C. DI water was pumped and induced at flow rates of 10 ml/min and 2 ml/min to the anode and cathode, respectively. The performance was evaluated by the chronoamperometry (CA) and the electrochemical impedance spectroscopy (EIS).

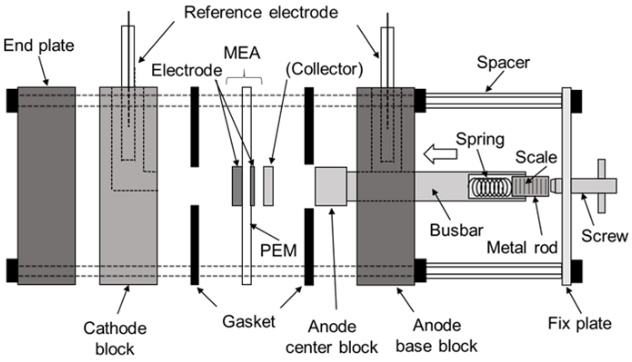

Fig. 1. PEM electrolyzer

Table. 1. Parameters of PTL

| Pore size/μm | Porosity/% | Thickness/mm |
|---|---|---|
| 600 | 87 | 2.5 |
| 600 | 85 | 1.5 |
| 600 | 85 | 1.0 |
| 600 | 84 | 0.5 |
| 300 | 85 | 1.0 |

## Results and discussion

Figure 2 shows the relationship between current density and anode and cathode potential obtained by polarization separation using double references. Colored plots are the measured potentials, and color framed plots are *iR*-free potentials. Therefore, the latter potentials are consisted of activation overpotential and mass transfer overpotential. As shown in upper part of Fig. 2, we obtained the anode mass transfer polarization by subtracting the Tafel line from the *iR*-free anode polarization. This anode mass transfer polarization proportional to the current density, so we obtained the mass transfer resistance by calculating its slope.

Figure 3 shows the relationship between PTL thickness and anode mass transfer resistance. The mass transfer resistance increased with the thickness of the PTL, and the slope of the mass transfer resistance also increased with the thickness. Thicker PTL might slow mass transportation of reactant and products in the catalyst layer because of slower linear velocity of water through the flow channel. Decreasing the pore size from 600μm to 300μm increased the mass transfer resistance. The impact of mass transfer associated with the narrow path of liquid-gas two phase flow and tortuosity due to the small pore size might affect mass transportation of reactant and products. However, 300μm pore PTL showed better cell performance.

Figure 4 shows the relationship between PTL pore size and anode mass transfer resistance, electrical resistance. 300μm pore PTL showed the smaller electrical resistance than 600μm pore PTL. We consider that the cause was the effect of electrical resistance in in-plane direction of CL. The small pore size was effective for electron transfer to improve CL utilization. Therefore, we consider that the cell performance was better at 300μm pore PTL due to the greater effect of smaller electrical collection resistance from the CL than that of mass transfer.

## Acknowledgment

This study was partially supported by the development of fundamental technology for advancement of water electrolysis hydrogen production in advancement of hydrogen technologies and utilization project (JPNP14021) commissioned by the New Energy and Industrial Technology Development Organization (NEDO) in Japan.

## References

[1] M. Carmo, D.L. Fritz, J. Mergel, D. Stolten, *Int. J. Hydrogen Energy*. **38,** 4901-4934 (2013).

[2] K. Nagasawa, T. Ishida, H. Kashiwagi, Y. Sano, S. Mitsushima, *Int. J. Hydrogen Energy*. 46, 36619-36628 (2021).

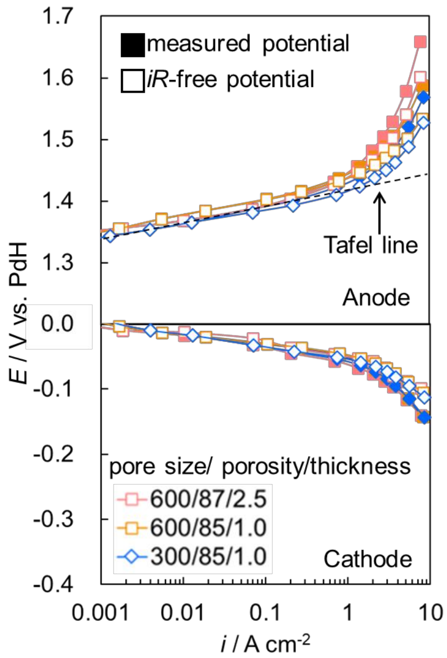

Fig. 2. Anode and cathode polarizations

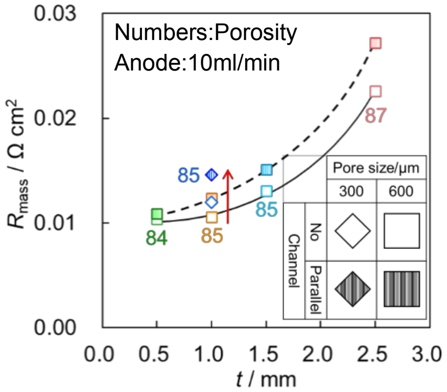

Fig. 3. Relationship between anode mass transfer resistance and PTL thickness

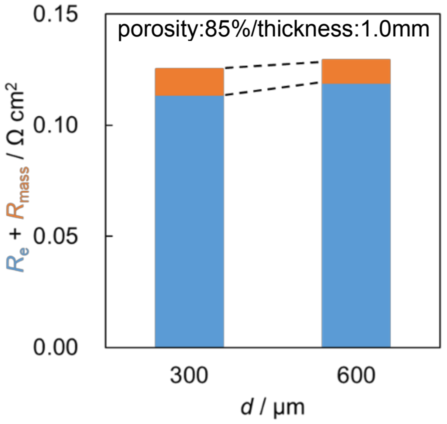

Fig. 4. Relationship between anode mass transfer resistance, electrical resistance and PTL pore size

P6

# THE EFFECT OF HYDROPHILIC CONTROL OF THE CATHODE FOR TOLUENE DIRECT-HYDROGENATION ELECTROLYZER

Daiki Kudo,[1] Kensaku Nagasawa,[2] Yoshiyuki Kuroda,[1,2] and Shigenori Mitsushima[1,2]

[1]*Graduate School of Engineering Science, Yokohama National University, 79-5 Tokiwadai, Hodogaya-ku, Yokohama 240-8501, Japan.*
[2]*Institute of Advanced Sciences, Yokohama National University, 79-5 Tokiwadai, Hodogaya-ku, Yokohama 240-8501, Japan.*
E-mail: ynugr-cel@ynu.ac.jp

**Keywords:**. Organic chemical hydride, Membrane electrolysis, Microporous layer

## INTRODUCTION

Introduction of renewable energy is expected to reduce carbon dioxide emissions. However, imbalance between the renewable energy supply and energy demand in regional and temporal is significant issue, and a system is required to store and transport electricity to convert into chemical energy like hydrogen. The toluene (TL)-methylcyclohexane (MCH) of chemical hydride system is one candidate for a hydrogen energy carrier. The advantage of this system is that the TL-MCH is liquid at ambient temperature and pressure and uses conventional petroleum infrastructure. We focus on direct electrolytic hydrogenation TL with water decomposition using proton exchange membranes (PEM) to improve MCH synthesis with two-step process of hydrogen production by water electrolysis and chemical hydrogenation of TL. In this system, water decomposes to oxygen and proton at the anode, the proton transports through the PEM, and TL hydrogenates to MCH with the proton at the cathode. Here, there is an issue that the electroosmotic drag water of proton through the PEM inhibits TL transportation and electrohydrogenation [1].

In this study, the hydrophobicity of cathode to improve Faraday efficiency has been investigated by enhancing water discharge from the cathode catalyst layer (CL) to improve TL mass transfer. In the cathode, We focused on the effect of the hydrophobicity of the microporous layer (MPL), which is between the CL and the carbon paper that works as backing of the CL and TL flow filed, by adding hydrophilic diatomite on the Faraday efficiency.

## EXPERIMENTAL

The anode was DSE® for oxygen evolution (De Nora Permelec Co., Ltd.), and the PEM was Nafion117® (DuPont). The cathode was three layer structure of CL/microporous layer (MPL)/porous carbon substrate. Mixture of Ketjen black (EC-300J, LION), a diatomite (157607, MP Biomedicals) and a PTFE dispersion (31-JR, Mitsui DuPont Fluorochemicals) was coated onto carbon paper (TGP-H-090H, Toray) to form the MPL on the carbon substrate. Weight ratio of diatomite in MPL were 0, 4, 8, 12, and 16 wt%. PtRu/C (TEC61E54, TKK) catalyst mixed with 5 % Nafion® dispersion (DuPont) was coated on the MPL. The cathode electrode and PEM were hot-pressed at 120°C and 4 MPa for 3 min to make a membrane electrode assembly (MEA).

Cathode and anode reactants were 10 mL min$^{-1}$ circulation of 10% TL-MCH and 1mol dm$^{-3}$ $H_2SO_4$, respectively. Operation temperature was 60ºC. The electrochemical measurements are chronoamperometry (CA), electrochemical impedance spectroscopy (EIS), and Faraday efficiency measurement. Faraday efficiency was determined with the volume ratio of generated hydrogen gas and toluene-methylcyclohexane solution obtained at the outlet of cathode chamber by Faraday's law.

## RESULT AND DISCUSSIONS

Figure 1 shows the internal resistance, the *IR*-corrected cell voltage and Faraday efficiency as a function of current density, respectively. The internal resistance was almost the same regardless of the diatomite addition. Therefore, the addition of the insulating diatomite in this range does not significantly increase the MPL resistivity. The addition of 8 wt% resulted in the lowest cell voltage and the highest Faraday efficiency. In addition, the cell voltage increased at the current density where the Faraday efficiency decreased. This would be due to the transition of the catalytic reaction from TL-hydrogenation to hydrogen generation.

Figure 2 shows the EIS at 1.7 V with the various diatomite addition with an inset of the equivalent circuit with the resistances: $R_1$, $R_2$ and $R_3$, and constant phase elements: $CPE_2$ and $CPE_3$. They represent the internal resistance, cathodic and anodic charge transfer resistances with each parallel constant phase element, which corresponds to higher and lower frequency semi-circles, respectively. The assignment of the equivalent circuit is based on the experiments with various operation conditions in our previous study[2]. The $R_3$ was almost the same for various diatomite addition and the analysis of $R_2$ corresponds to mass transfer in the cathode catalyst layer.

Figure 3 shows the current density at 90% of Faraday efficiency and the $R_2$ of the cathodic charge transfer resistance at 1.7 V as a function of weigh ratio of diatomite in the MPL. The addition of 8 wt% resulted in the highest current density at 90% of Faraday efficiency and the lowest cathodic charge transfer resistance. The reduction in cathodic charge transfer resistance indicating that Improved TL mass transfer by hydrophilic diatomite becoming an outlet path for water. This improved Faraday efficiency.

## ACKNOWLEGEMENTS

This work was based on results obtained from the Development of Fundamental Technology for Advancement of Water Electrolysis Hydrogen Production in Advancement of Hydrogen Technologies and Utilization Project (JPNP14021) commissioned by the New Energy and Industrial Technology Development Organization (NEDO). The anode was supplied by De Nora Permelec Ltd. We appreciate the person concerned them.

## REFERENCES

[1] K. Nagasawa, K. Tanimoto, J. Koike, K. Ikegami, S. Mitsushima, *J. Power Sources*, 439, 227070 (2019).
[2] K. Nagasawa, A. Kato, Y. Nishiki, Y. Matsumura, M. Atobe, S. Mitsushima, *Electrochimica Acta*, 459-465, 246 (2017).

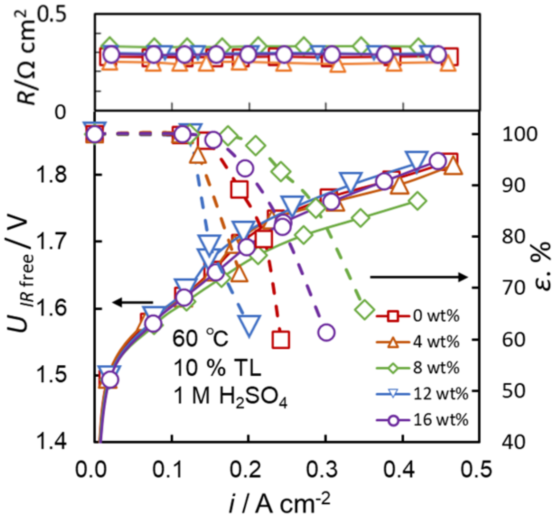

Fig.1 Cell voltage (solid lines), Faraday efficiency (dashed lines) and internal resistance as a function of current density with various weight ratio of diatomite

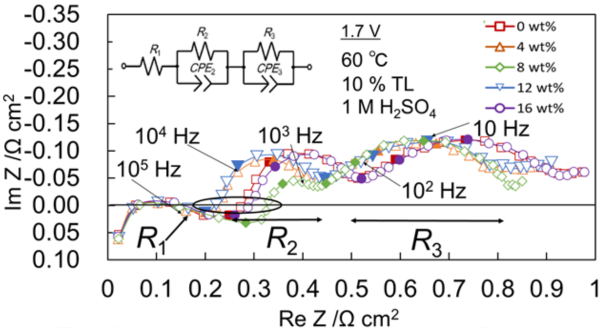

Fig.2 Impedance spectra at 1.7 V with various weight ratio of diatomite

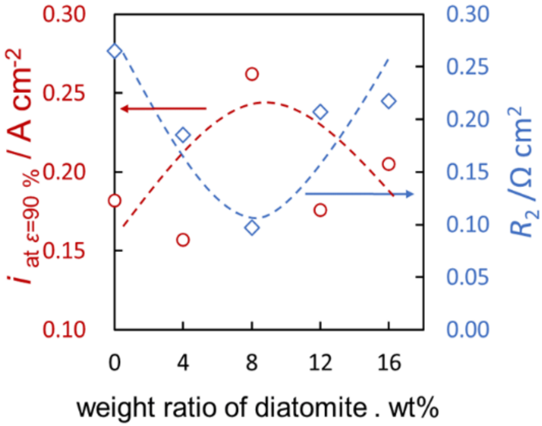

Fig.3 Current density at ε=90% (left side) and Cathodic reaction resistance at 1.7V (right side) as a function of weight ratio of diatomite

P7

# Performance Evaluation and Analysis of Bubble Detachment Factors for Alkaline Water Electrolyzer

Kazuyuki Matsukawa[1], Yoshiyuki Kuroda[1,2], Takahiro Higashino[3], Kazuki Okuno[3], Hiromasa Tawarayama[3], Akihisa Hosoe[3] and Shigenori Mitsushima[1,2]

[1] Grad. School of Eng. Sci., Yokohama Natl. Univ., 79-5 Tokiwadai, Hodogaya-ku, Yokohama, 240-8501, Japan

[2] IAS, Yokohama Natl. Univ., 79-5 Tokiwadai, Hodogaya-ku, Yokohama, 240-8501, Japan

[3] Energy and Electronics Materials Laboratory, Sumitomo Electric Industries, Ltd., 1-1-1, Koyakita, Itami, Hyogo, 664-0016, Japan

**Keywords:** Alkaline water electrolysis, Gas bubble, Oxygen evolution reaction, Foam electrode, Oscillation analysis

## INTRODUCTION

Toward the realization of a hydrogen society without any carbon dioxide emission, water electrolysis to produce hydrogen using renewable electricity is attracting attention. Alkaline water electrolysis (AWE) is one of the water electrolysis technologies, which uses low-cost materials. To reduce hydrogen production cost, further cost reduction with current density increase is needed . To increase the current density using porous electrodes by removing bubble through liquid flow and other ways have been attempted[1]. On the other hand, bubble behavior inside porous electrodes, which is difficult to observe, is not well understood. In this study, we analyzed factors related to bubble detachment with Ni foam electrodes, and evaluated the impact of bubble detachment on performance. Especially, this study focused on potential oscillation with constant current measurement in different flow rates and pressure conditions.

## EXPERIMENTAL

We utilized the forced-flow alkaline electrolyzer with the Ni porous material(pore size 0.45 mm, thickness 1 mm) as anode and cathode, which also serves as electrolyte flow path. Reference was SSCE in saturated KCl solution, and separator was Zirfon®(AGFA, thickness 500 μm). Electrolyte is 7M KOH solution at 303 K.

After pre-treatment, the effect of flow rate on the activity was evaluated with chronopotentiometry in the current range from 0.5 to 250 A $F^{-1}$ under flow rate 10 to 100 mL/min in pressurized same experiments were conducted for liquid pressurization conditions of 0.1 to 0.3 MPa.

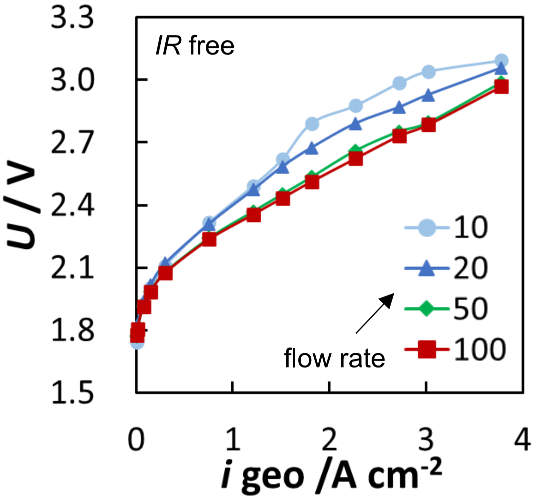

Fig. 1 Polarization curves for flow rate of 10-100 mL/min.

## RESULTS AND DISCUSSION

Figure 1 shows the polarization curves for various on flow rate. Increase of the flow rate reduced the cell voltage, especially in high current density region above 1.5 A $cm^{-2}$. Figure 2 shows the potential changes at 1.5 A $cm^{-2}$ by discrete Fourier transform with inset of potential vibration as a function of time. Vertical axis is amplitude of the potential vibration and horizontal axis is frequency of the oscillation. A large peak is observed around 1 Hz for the flow rate of 10 and 20 mL/min, which corresponds to oscillation of 1 second cycle. Increase of the flow rate from 10 to 20 mL/min shifted the peak frequency from 0.92 to 1.29 Hz. The large oscillation would be caused by bubbles growth, detachment and coalescing in the foam electrode[2]. In high flow rates, the bubbles would discharge from the electrode in a short cycle, which shifted the peak to the high-frequency and led to a reduction in cell voltage.

Figure 3 shows the polarization curves for various pressure. Increase of pressure reduced the cell voltage, especially in high current density region above 1.5 A cm$^{-2}$. Figure 4 shows the potential oscillation at 1.5 A cm$^{-2}$ at flow rate of 10 mL/min. The large peaks around 1 Hz shifted the peak from 1.62 Hz to 0.45 Hz with the pressure increase from 0.1 to 0.3 MPa. Higher pressure showed slower the growth rate of bubbles, because of higher mole density per unit volume. Therefore, smaller bubble with low frequency would be enough for certain current at higher operating pressure.

As described above, oscillation analysis has enabled the analysis of bubble behavior, which is difficult to visualize, such as in a porous electrode.

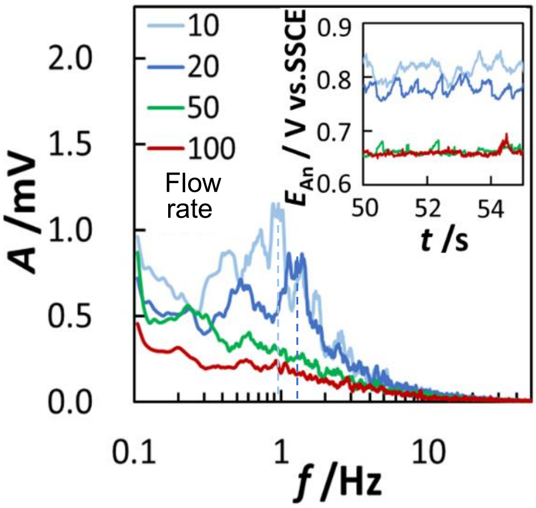

Fig. 2 Oscillation analysis of potential change for flow rate of 10-100 mL/min.

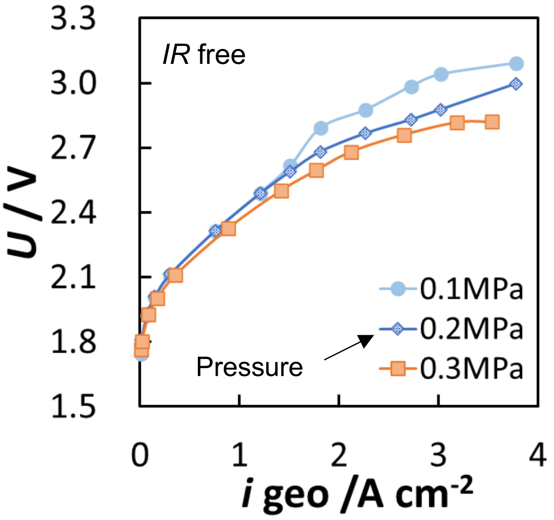

Fig. 3 Polarization curves for pressure of 0.1-0.3 MPa.

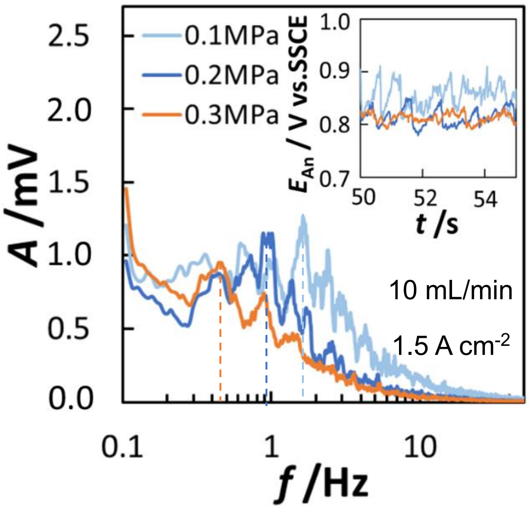

Fig. 4 Oscillation analysis of potential change for pressure of 0.1-0.3 MPa.

## ACKNOWLEDGEMENTS

A part of this study was based on results obtained from the Development of Fundamental Technology for Advancement of Water Electrolysis Hydrogen Production in Advancement of Hydrogen Technologies and Utilization Project (JPNP14021) commissioned by the New Energy and Industrial Technology Development Organization (NEDO).

## REFERENCES

[1] F. Yang, M. J. Kim, M. Brown, B. J. Wiley, *Advanced Energy Materials*, **10**, 2001174(2020)

[2] C. Gabrielli, F. Huet, R. P. Nogueira, *Electrochimica Acta*, **50**, 3726-3736(2005)

P8

# FRACTAL DESIGN OF FLOW FIELD PLATE FOR PEMFC

Abdelhakim Merdjani[1], a, Natalia Kizilova[1],

[1]Warsaw University of Technology, Poland, abdelhakim.merdjani.dokt@pw.edu.pl.

**Keywords:** Fuel cells, flow field plate, fractal distributor

## INTRODUCTION

Fuel cells (FC) are perspective sources of green energy for industry and domestic use. In the proton exchange membrane (PEM) FC the electric energy is directly converted from hydrogen oxidation reaction at the catalyst layer [1,2]. The gas fuels H2 and O2 are pumped through a system of channels in the flow-field plate (FFP) and delivered to the PEM through the porous gas diffusion layer (GDL). The FFP occupy ~90% of the volume and ~80% of the mass of a FC stack. Therefore, many efforts were exerted to FFP optimization for gas delivery at low pumping pressure and weight and high durability.

The conventional FFP designs are formed by open channels that are in contact with GDL. The serpentine-type FFPs are considered as golden standard for comparative testing of novel designs. They have high hydraulic resistivity $Z_h$ and non-uniform fuel distribution but low water flooding of the channels. Other types of the conventional FFPs have lower $Z_h$, more uniform fuel delivery but they are vulnerable for water accumulation. Therefore, the best FFP design can be done by the multicriteria optimization approach.

nowadays the flow field design is being developed continuously from conventional to modified and hybrid like bio-inspired designs figure1

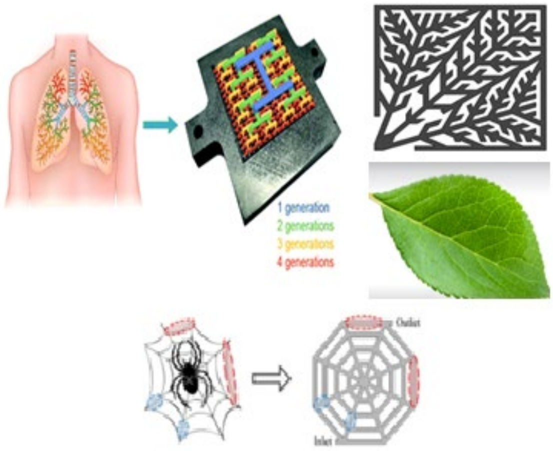

Figure1.bio-inspired examples of flow field plate in FC

## Methods.

The fractal system of rectangle channels (figure2) provided uniform fuel delivery at low hydraulic resistivity, viscous and thermal dissipation is proposed based on the CFD simulations. The fractal channels are not open into the GDL and the mass flow is provided via the open outlets of the smallest channels only. When the outlets are uniformly distributed over PEM, the homogeneous fuel delivery is granted. Geometry of the fractal was determined by the minimum entropy generation due to viscous dissipation (isothermal case) [2] that had been tested experimentally in the FC stacks [3].

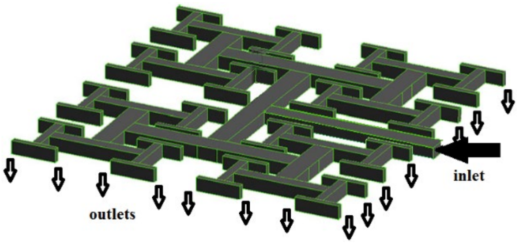

Figure 2. Geometry of the fractal distributor

The table below show comparative study of flow field plate efficiency

| Flow field type | FFP dimension (cm) | Pressure drop | Current density (A/cm$^2$) | ref |
|---|---|---|---|---|
| T-type Fractal | 5*5 | 0.5 bar | 1.8 | [3] |
| Simple serpentine | 7*7 | ~ 1bar | <1 | [4] |
| Double serpentine | 7*7 | ~ 1 bar | <1 | [4] |

**Conclusion**

The bio design was shown to have lower pressure losses which allowed it to produce 2-3 times better power output per pumping power input than the parallel design, while also maintaining better reactant distribution

## REFERENCES

[1] SAZALIS, N., WAN SALLEH, W. N., JAMALUDIN, A. S., & MHD RAZALI, M. N. (2020). New perspectives on fuel cell technology: A brief review. Membranes, 10(5), 99

[2] SAUERMOSER, M., KJELSTRUP, S., KIZILOVA, N., POLLET, B. G., & FLEKKOY, E. G. (2020). Seeking minimum entropy production for a tree-like flow-field in a fuel cell. Physical Chemistry Chemical Physics, 22(13), 6993-7003

[3] SAUERMOSER, M., POLLET, B. G., KIZILOVA, N., & KJELSTRUP, S. (2021). Scaling factors for channel width variations in tree-like flow field patterns for polymer electrolyte membrane fuel cells-An experimental study. international journal of hydrogen energy, 46(37), 19554-19568.

P9

# FORMATION OF METAL HYDROXIDE-BASED COMPOSITE ANODE CATALYSTS FOR ALKALINE WATER ELECTROLYSIS VIA CO-ELECTRODEPOSITION OF HYBRID COBALT HYDROXIDE NANOSHEETS

Daiji Mizukoshi,[1] Tatsuya Taniguchi,[2] Yuta Sasaki,[2] Yoshinori Nishiki,[3] Zaenal Awaludin,[3] Takaaki Nakai,[3] Akihiro Kato,[3] Shigenori Mitsushima,[1,4] Yoshiyuki Kuroda[1,4]
[1]Grad. School of Eng. Sci., Yokohama Natl. Univ., 79-5 Tokiwadai, Hodogaya-ku, Yokohama 240-8501, Japan
[2]Kawasaki Heavy Ind., Ltd., 1-1 Kawasakicho, Akashi, Hyogo, 673-8666, Japan
[3]De Nora Permelec, Ltd., 2023-15 Endo, Fujisawa, Kanagawa, 252-0816, Japan
[4]Adv. Chem. Energy Res. Center, Inst. of Adv. Sci., Yokohama Natl. Univ., 79-5 Tokiwadai, Hodogaya-ku, Yokohama 240-8501, Japan
E-mail: ynugr-cel@ynu.ac.jp

**Keywords:** Co-deposition, Alkaline water electrolysis, Renewable energy, Self-repairing catalyst, Nanosheet, Nanorod, OER activity

## INTRODUCTION

When an alkaline water electrolyzer is powered by fluctuating renewable energy, electrode degrades rapidly due to reverse current[1]. We have reported a concept of self-repairing catalysts, where a catalyst dispersed in the electrolyte is self-assembled on the electrode to repair a degraded catalyst layer[2]. We proposed one of the self-repairing catalysts, hybrid hydroxide cobalt nanosheet (Co-ns), consisting of a brucite-type cobalt hydroxide nanosheet modified with a tripodal ligand on the surface. Nickel electrodes coated with Co-ns exhibited quite high durability under potential cycling conditions. We also have reported another catalyst, β-FeOOH nanorod (FeOOH-nr). Although it has self-repairing ability during oxygen evolution reaction (OER), the amount of deposition is smaller than that of Co-ns, and a multitude of self-repairing operation is necessary. Here, we demonstrate the mixed catalysts, composed of Co-ns and FeOOH-nr. These composite catalysts act as self-repairing catalyst and the OER catalyst with high activity. In this study, we investigated their OER activity, the amount of deposition of both cobalt and iron, and the mechanism of how the amount of deposited iron increased.

## EXPERIMENTAL

Co-ns[2] and FeOOH-nr[3] was synthesized according to the literature. Electrochemical tests were performed in a 1.0 M KOH, using a PFA three-electrode cell. A nickel plate, a nickel coil, and a reversible hydrogen electrode (RHE) were used as the working, counter, and reference electrodes, respectively. The Co-ns dispersion, FeOOH-nr dispersion, or their mixture (total concentration of catalyst weights = 80 ppm) was added in the electrolyte. Catalysts were deposited by the following processes according to our previous report[2]. The following processes were repeated for 10 times: i) chronopotentiometry (CP) at 800 mA cm$^{-2}$ for 30 min, ii) cyclic voltammetry (CV) between 0.5 and 1.8 V vs. RHE at 5 mV s$^{-1}$, iii) CV between 0.5 and 1.6 V vs. RHE at 50 mV s$^{-1}$, iv) electrochemical impedance spectroscopy (EIS) at 1.6 V vs. RHE with the frequency range 0.1－$10^5$ Hz. Elemental analysis of β-FeOOH-nr was performed by inductively coupled plasma atomic emission spectroscopy (ICPAES)using an SII SPS3000 spectrometer. The samples were dissolved in hydrochloric acid for measurements. A catalyst deposited on a nickel electrode was dissolved in a 1M HCl aq. and then diluted to 0.1M HCl aq. for the measurement. Transmission electron microscopy (TEM) images were recorded using a JEOL JEM-2100F microscope at the accelerating voltage 200 kV. The samples were dispersed in ethanol and dried on a holey carbon-coated Cu microgrid.

## RESULTS AND DISCUSSION

The OER polarization curves during the repeated electrolysis are shown in the Fig. 1. The OER activity of the electrodes were improved by mixing Co-ns and FeOOH-nr. When the mixed catalysts were used as OER catalyst, the OER overpotential at 100 mA cm$^{-2}$ ($\eta_{100}$) was 302 mV after 10th cycle of the repeated electrolysis. However, when FeOOH-nr and Co-ns were used as OER catalyst, the OER overpotentials at 100 mA cm$^{-2}$ ($\eta_{100}$) were 310 mV and 353 mV, respectively, after 10th cycle of the repeated electrolysis.

Furthermore, the repeated electrochemical tests were conducted using the mixed catalysts with various ratio of the concentration of FeOOH-nr and Co-ns. The correlation of the deposited amount of Co, and the deposited amount of Fe and the OER performance of the mixed catalysts is shown in the Fig. 2. The deposited amount of Fe, using the composite catalysts, were larger than that of FeOOH-nr only. When 40 ppm of FeOOH-nr dispersion and the same concentration of Co-ns dispersion was used as OER catalysts, the deposited amount of Fe was 26.5 μg cm$^{-2}$. On the contrary, when only FeOOH-nr was used as OER catalyst, the amount of deposited Fe was 2.00 μg cm$^{-2}$. This increase in the FeOOH-nr is well correlated with the improved OER activity.

After the electrolysis, the composite structure of FeOOH-nr and Co-ns was observed using TEM (Fig. 3). It was found that rodlike shape of FeOOH-nr was surrounded by the two-dimensional shape of Co-ns. It was suggested that Co-ns made FeOOH-nr easier to deposit on the electrode due to the forming of composite aggregates in the electrolyte.

In conclusion, it was found that the amount of deposition of FeOOH-nr on the electrode was successfully increased by the co-deposition with Co-ns, using the mixed catalysts and this phenomenon contributed to the higher OER activity. This finding implies that it is possible to use highly active catalysts without self-repairing ability as a self-repairing catalyst.

## ACKNOWLEDGEMENTS

This work was supported partially by the JSPS KAKENHI from MEXT, Japan.

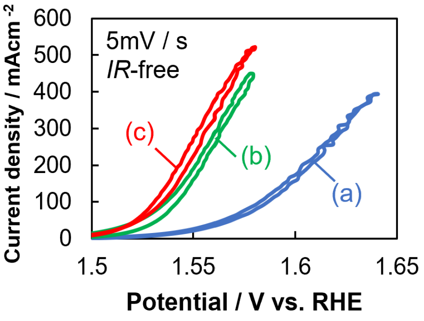

Fig. 1 Polarization curves of (a) Co-ns, (b) FeOOH-nr, and (c) mixed catalyst coated on Ni electrodes.

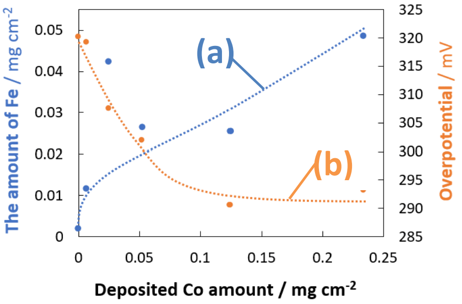

Fig. 2 (a) The amount of Fe and (b) OER overpotential as a function of deposited Co amount

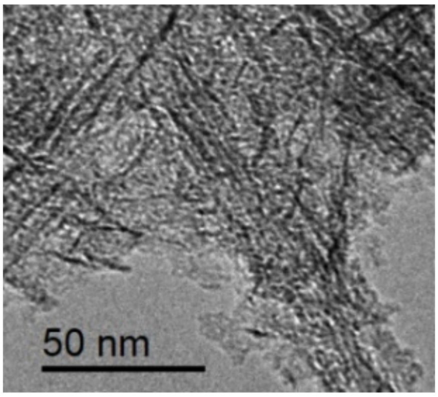

Fig. 3 TEM image of the mixed catalyst layer

## REFERENCES

[1] Y. Uchino *et al*., *Electrocatalysis* **9**, 67 (2018).
[2] Y. Kuroda *et al*., *Electrochim. Acta.* **323**, 1348122 (2019).
[3] Y. Kuroda *et al*., *J. Sol-Gel Sci. Technol*., in press

P10

# Relationship between Faraday efficiency and drag water for electrochemical toluene hydrogenation

Shota Oi,[1] Kensaku Nagasawa,[2] Yoshiyuki Kuroda,[1, 2] and Shigenori Mitsushima[1, 2]

[1]*Graduate School of Engineering Science, Yokohama National University, 79-5 Tokiwadai, Hodogaya-ku, Yokohama 240-8501, Japan.*
[2]*Institute of Advanced Sciences, Yokohama National University, 79-5 Tokiwadai, Hodogaya-ku, Yokohama 240-8501, Japan.*
E-mail: cel@ml.ynu.ac.jp

**Keywords**: Organic hydride, Electrochemical toluene hydrogenation, Drag water, Electro-osmosis, Back diffusion, Faraday efficiency

## INTRODUCTION

To decrease carbon dioxide emissions, utilization of renewable energy must be major primary energy source. Here, imbalance between supply and demand in space-time is significant issue. Therefore, the large-scale storage and transportation of hydrogen as secondary energy is needed for effective utilization. Toluene (TL) / methylcyclohexane (MCH) organic hydride system is one of the best candidates of hydrogen energy carrier, because TL and MCH are liquid at ambient temperature and pressure, and it would be able to use petroleum infrastructure. To improve the energy conversion efficiency for TL hydrogenation using renewable electricity, we have studied direct electro-hydrogenation of TL with water decomposition using proton exchange membrane (PEM). The rate-determining step for the cathode is the mass transfer of TL to the catalyst layer (CL) [1]. One of the major factors inhibiting TL transportation to the cathode catalyst is electro-osmotic drag water from the anode through the PEM. The drag water that transports into the cathode CL inhibits the TL transportation and decrease the Faraday efficiency.

In this study, the influence of water flux through the PEM on Faraday efficiency by changing sulfuric acid concentration of anolyte was evaluated to improve Faraday efficiency for electrochemical TL hydrogenation.

## EXPERIMENTAL

A DSE® (De Nora Permelec, Ltd.) for the oxygen evolution, which is a titanium mesh electrode coated electrocatalyst, and Nafion 117® (Du Pont) were used as the anode and PEM, respectively. Carbon paper (10BC, SGL carbon ltd.) loaded with $0.7\ \mathrm{mg_{\text{-PtRu}}\ cm^{-2}}$ of PtRu/C (TEC61E54, Tanaka Kikinzoku Kogyo) was used as the cathode. The cathode was hot-pressed on the PEM at 120°C and 4 MPa for 3 min to fabricate a membrane cathode assembly (MEA).

During electrolysis, cathode reactant of 10% or 100% TL diluted by MCH, and anode reactant of 0-1.5 M (= mol $\mathrm{dm^{-3}}$) $H_2SO_4$ were circulated at 10 mL $\mathrm{min^{-1}}$. Operation temperature was 60°C. As electrochemical measurements, chronoamperometry, electrochemical impedance spectroscopy, Faraday efficiency measurement and water flux measurement were conducted. Faraday efficiency was determined with the volume ratio of generated hydrogen gas and TL-MCH solution obtained at the outlet of cathode chamber by Faraday's law. Water flux was determined with the weight of water discharged from the outlet of cathode chamber during chronopotentiometry.

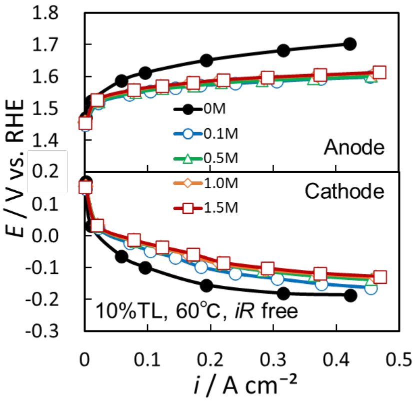

Fig. 1 *iR* corrected anode and cathode polarization curves.

## RESULTS AND DISCUSSION

Figure 1 shows *iR* corrected the anode and the cathode polarization curves. There was no significant difference in polarization curves except for 0 M. Here, the DSE® for the oxygen reaction is a mesh electrode which is used in electrolyte. Therefore, at 0 M, the active area is limited at the interface between anode and membrane, and the anode was polarized. During these experiments, discharged water from the outlet of the cathode chamber was sulfuric acid whose concentration was about one-tenth that of the anolyte. Therefore, at 0M, the effective surface area of the cathode catalyst would also have been decreased.

Figure 2 shows relationship between water flux and current density at various sulfuric acid concentrations. The water flux decreased as the increase of the anolyte concentration except for 0 M. This would be back diffusion toward electro-osmosis due to increase of anolyte concentration.

Figure 3 shows Faraday efficiency as a function of current density at various sulfuric acid concentrations for 10% and 100% TL. For 10% TL, there was no significant difference in Faraday efficiency. Low concentration of TL limited TL transfer into CL and the effect of drag water on the Faraday efficiency would not be significantly. On the other hand, the Faraday efficiency of 100% TL decreased in higher current density region, and the onset current density of the Faraday efficiency decrease increased with the anolyte concentration.

To discuss Faraday efficiency, we should consider microlevel mass balance in the CL, which determine local concentration of TL, but overall mass balance was discussed. In a steady state without hydrogen evolution, inlet and outlet flux must be same.

$$J_{TL} + J_{H2O,\ in} = J_{MCH} + J_{H2O,\ out}$$

Here, $J_{TL}$, $J_{H2O,\ in}$, $J_{MCH}$, and $J_{H2O,\ out}$ are TL flux into the CL with diffusion, water flux into the CL with electro-osmosis, MCH formation with hydrogenation, and water flux from the CL with diffusion, respectively. The electro-osmosis and MCH formation would correspond to electrochemical reaction and the diffusion factors would be affected by effective diffusion coefficient as a function of pore structure and wettability of the CL. Therefore, local concentration would be controlled by the design of the CL, but overall mass balance must be $J_{TL} = (M_{TL}/M_{MCH})J_{MCH}$ and $J_{H2O,\ in} = J_{H2O,\ out}$. $M_{TL}$ and $M_{MCH}$ are molecular weight of TL and MCH, respectively. Here, as a criterion to evaluate Faraday efficiency, overall flux of water and MCH, which disturbed TL transportation, was discussed in Fig. 4.

Figure 4 shows the onset current density of the Faraday efficiency decrease for 100% TL as a function of $J_{MCH}$, $J_{H2O}$ and $J_{H2O+MCH}$. $J_{MCH}$ was calculated by Faraday's law and $J_{H2O}$ was obtained by interpolation of Fig. 2 as overall flux. The onset current density was observed at almost constant $J_{H2O+MCH}$. This indicates that effective diffusion coefficient would have been constant due to using the same MEA, thus Faraday efficiency would have been affected by $J_{H2O+MCH}$.

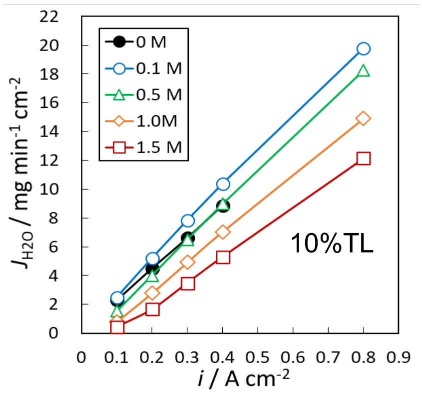

Fig. 2 Relationship between water flux and current density at various sulfonic acid concentrations.

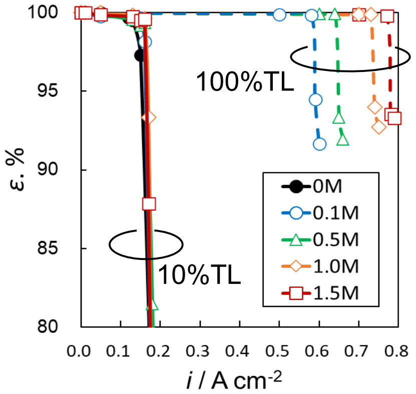

Fig. 3 Faraday efficiency as a function of current density at various sulfuric acid concentrations.

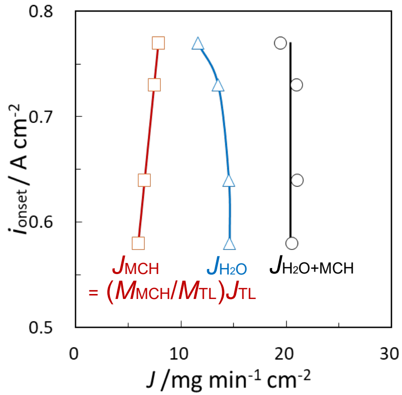

Fig. 4 The onset current density of the Faraday efficiency decrease for 100% TL as a function of $J_{MCH}$, $J_{H2O}$ and $J_{H2O+MCH}$.

## ACKNOWLEDGEMENTS

This work was based on results obtained from the Development of Fundamental Technology for Advancement of Water Electrolysis Hydrogen Production in Advancement of Hydrogen Technologies and Utilization Project (JPNP14021) commissioned by the New Energy and Industrial Technology Development Organization (NEDO). The anode was supplied by De Nora Permelec Ltd. We appreciate the person concerned them.

## REFERENCES

[1] K. Nagasawa, Y. Sawaguchi, A. Kato, Y. Nishiki, S. Mitsushima, *Electrocatalysis*, 8, 164 (2017).

# Polyaniline coating of carbon to increase corrosion resistance

Nikhat Pasha, Grandi Maximilian, Victor Hacker

Nikhat Pasha, Tu Graz, Austria, nikhat.pasha@student.tugraz.at ; Grandi Maximilian, Tu Graz, maximilian.grandi@tugraz.at

## Abstract

PANI (polyaniline) is a conductive polymer with a certain amount of diaminobenzenoid and diiminoquionoid rings. It belongs to an important family in the conducting polymers with diverse applications such as chemically modified electrodes, plastic batteries, corrosion protection. Although, this class of polymer was discovered 150 years ago, it has attracted the attention of many scientists, mainly due to the discovery of the high electrical conductivity of PANI [1]. High conductive polyaniline (PANI) has properties of high conductivity, low cost, high flexibility, ease of synthesis, environmental friendliness, and has a unique redox property that has been used in the storage of electrochemical energy and conversion technologies which include supercapacitors, rechargeable batteries, and fuel cells. Its conductivity has shown better performance in the supercapacitors, rechargeable batteries, and fuel cells [1].

In this study, different strategies and modification techniques are used to optimize the PANI for specific applications. Synthesis of PANI was studied and several methods were examined, as it is simple. Chemical oxidative polymerization is the oldest and most used method for the synthesis of PANI in bulk quantities. The mechanism, the chemical method, the electrochemical polymerization of aniline and its derivatives and the kinetics of the oxidative polymerization are outlined. However, PANI/Pt shows good catalytic behavior. The main problem is the agglomeration of carbon particles and the slow charge that blocks its application. Also, Pt is very expensive, and this limits its commercial utilization. Many Pt – free non noble metal – based catalysts have been identified as catalysts with high ORR activity.  Therefore, the aim is to optimize the catalyst to increase its lifetime and the activity. Als, the polyaniline coating of carbon was studied to increase the corrosion resistance without using problematic transition metals.

## Reference

[1] Li Z, Gong L. Research Progress on Applications of Polyaniline (PANI) for Electrochemical Energy Storage and Conversion. Materials (Basel). 2020 Jan 23;13(3):548. doi: 10.3390/ma13030548. PMID: 31979286; PMCID: PMC7040733.

P12

# HALF-CELL MEASUREMENTS OF PALLADIUM-BASED CATALYSTS FOR ETHANOL OXIDATION

ROSCHGER Michaela[1], WOLF Sigrid[1], HASSO Richard[1] and HACKER Viktor[1]

[1]TU Graz, Institute of Chemical Engineering and Environmental Technology, Inffeldgasse 25/C, 8010 Graz, Austria, michaela.roschger@tugraz.at

**Keywords:** alkaline direct ethanol fuel cell, half-cell measurement, gas diffusion electrode, cyclic voltammetry.

## INTRODUCTION

Alkaline direct ethanol fuel cells (ADEFCs) have received much attention for environmentally friendly power generation because the fuel, ethanol (Figure 1), is renewable, has low toxicity and high energy density, and is easily transportable and storable as a liquid fuel. The main challenge with ADEFC is the incomplete ethanol oxidation reaction (EOR) at the anode. Instead of forming 12 $e^-$, water, and $CO_2$ upon complete reaction, only 4$e^-$, acetic acid, or acetate are formed with currently available catalysts because the C-C bond cannot be completely cleaved. [1]

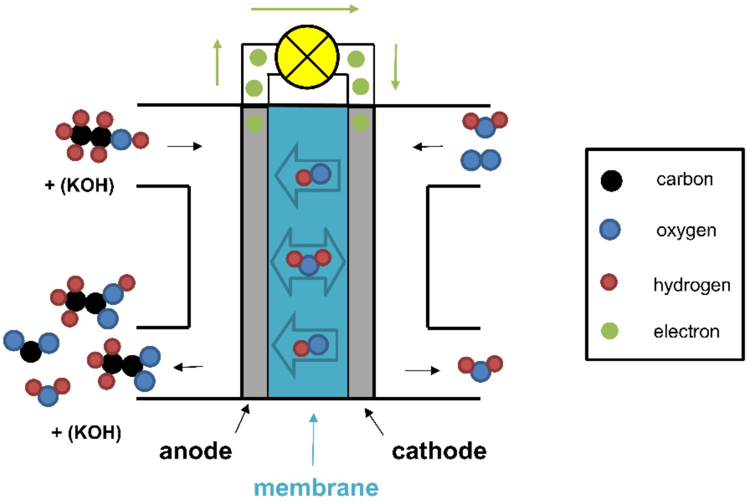

Fig. 1: Schematic illustration of the working mechanism of an ADEFC.

Electrochemical measurement methods such as cyclic voltammetry or chronoamperometry can be used to determine the activity, reactivity, stability of the anode catalyst. Most often, the rotating disk electrode (RDE) measurement method is used to determine these parameters (Figure 2). It has been shown that by using half-cell tests (Figure 2) with developed electrodes, the performance in the fuel cell and the influence of the three-phase boundary can be predicted. [2] In this study, we demonstrate the use of half-cell measurements to determine the EOR activity of the anode catalyst.

## EXPERIMENTAL

For the electrochemical half-cell measurements, electrodes were prepared by using an ultrasonic spraycoater from SONO-TEK® to deposit the catalyst uniformly on the carbon cloth gas diffusion layer (GDL). The ink consisted of a PdNiBi/C anode catalyst [3], isopropanol, water and ion-exchange ionomer. The produced electrodes were then characterized by using a Diskfix gas diffusion substrate holder with a flow field in a three-electrode half-cell arrangement. The oxidation and reduction behaviour of the catalysts were measured by cyclic voltammetry in potassium hydroxide solution. The

EOR measurements were performed using ethanol as reactant. A potentiostat from Zahner-elektrik GmbH&Co KG® was implemented for all electrochemical measurements.

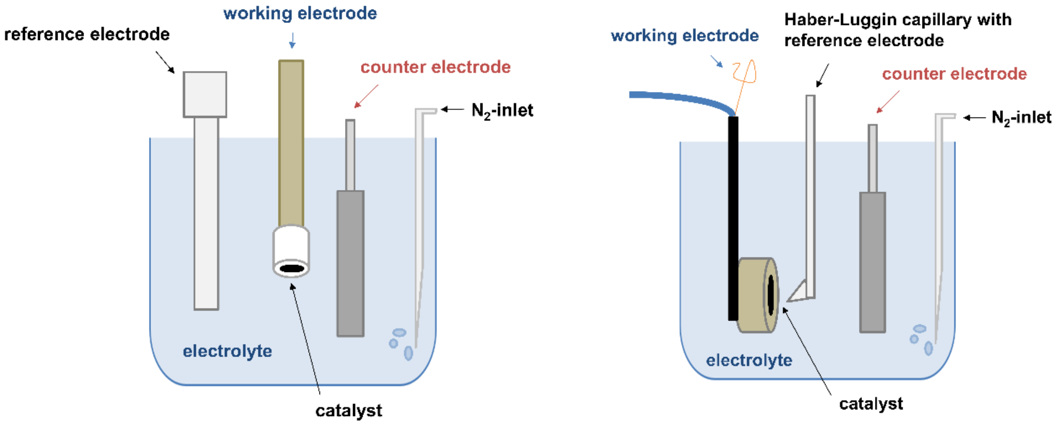

Fig. 2: Comparison of measurement setup for RDE (left) and half-cell tests (right).

## RESULTS

The cyclic voltammograms of the prepared PdNiBi/C electrodes show the characteristic oxidation and reduction peaks for all incorporated metals. The effect of temperature and concentration of KOH and EtOH on the performance of the electrode are discussed based on the results of EOR half-cell evaluation of PdNiBi/C catalyst in the poster presentation.

## ACKNOWLEDGEMENT

The authors acknowledge the financial support by the Austrian Science Fund (FWF): I 3871-N37.

## REFERENCES

[1] B.Cermenek, J.Ranninger, V.Hacker; In Ethanol: Science and Engineering, A.Basile, A.Iulianelli, F.Dalena, N.T.Veziroglu, Eds.; Elsevier Inc.: Amsterdam, 2019, 383-405.
[2] R. Loukrakpam, B. F. Gomes, T. Kottakkat, C. Roth, J. Phys. Mater., 2021, 4, 0044004.
[3] B. Cermenek, B. Genorio, T. Winter, S. Wolf, J.G. Connell, M. Roschger, I. Letofsky-Papst, N. Kienzl, B. Bitschnau, V. Hacker, Electrocatalysis, 2020, 11, 203–214.

P13

# ENHANCED $H_2$ BUBBLE REMOVAL FROM CATHODE OF ALKALINE WATER ELECTROLYZER BY COATING WITH HYDROPHILIC HYBRID MAGNESIUM HYDROXIDE NANOSHEET

Taiki Sano[1], Yoshiyuki Kuroda[1,2], and Shigenori Mitsushima[1,2]

[1]*Graduate School of Engineering Science, Yokohama National University, 79-5 Tokiwadai, Hodogaya-ku, Yokohama 240-8501, Japan.*
[4]*Institute of Advanced Sciences, Yokohama National University, 79-5 Tokiwadai, Hodogaya-ku, Yokohama 240-8501, Japan.*
E-mail: ynugr-cel@ynu.ac.jp

**Keywords:** alkaline water electrolysis, hydrophilic surface, hydrogen evolution reaction, nanosheet, renewable energy

## INTRODUCTION

Hydrogen has attracted much attention because of their usefulness as energy carrier for unstable renewable energy. Alkaline water electrolysis is one of useful hydrogen production processes, and it has advantages of a simple structure, the possibility of large-scale production, and the use of relatively inexpensive electrode materials [1]. However, because of the low electrode potential of the cathode during the hydrogen evolution reaction (HER), surface oxides are easily reduced to metal on the surface. It likely makes the electrode surface hydrophobic, which is disadvantageous for bubble removal [2]. To improve the wettability of the electrode surface and the ability for bubble release, we focused on a magnesium hydroxide as a hydrophilic surface coating. Because of the equilibrium potential of $Mg^{2+} + 2e^- \rightarrow Mg$ is quite low [3], the reduction of magnesium hydroxide during HER is negligible. Magnesium hydroxide is stable under alkaline conditions [4]. Recently, nanosheet of magnesium hydroxide has been prepared for the first time by the modification with organic compounds, which enables the coating of an electrode with a very thin layer of magnesium hydroxide. In this study, we investigated the HER behaviour of nickel electrodes coated with thin layer of hybrid magnesium hydroxide nanosheets on the basis of bubble removal.

## EXPERIMENTAL

A hybrid magnesium hydroxide nanosheet (Mg-ns) was synthesized according to the previous report [5]. To observe AFM image, Mg-ns was supported on a Si wafer preliminary washed with tetramethylammonium hydroxide solution [5]. Electrochemical measurements were performed using a three-electrode cell made of PFA. A Ni plate for the working electrode was etched with boiling 6 M HCl, followed by plasma treatment for hydrophilization and spin-coating (1500 rpm, 60 s) of Mg-ns dispersed in a mixture of water and ethanol (water : ethanol = 1 : 4). The spin-coating was repeated for 5, 10, 20, 30, and 50 times to vary the amount of Mg-ns. The measurements were performed using a reversible hydrogen electrode (RHE) as the reference electrode, a Ni coil as the counter electrode, and a 1.0 M KOH solution at 25°C as the electrolyte solution. First, (1) chronoamperometry (CA) (–0.5 V vs. RHE, 3 min) was performed to remove nickel oxides from the working electrode to evaluate the real surface area of Ni, and (2) cyclic voltammetry (CV) (0.1 to –1.0 V vs. RHE, 50 mV $s^{-1}$, 3 cycles) was performed, and (1) and (2) were repeated until the oxidation peak area became constant. The real surface area was evaluated from the peak area, assuming 0.514 mC $cm^{-2}$ [2]. Subsequently, CV (–1.0 ~ 0 V vs. RHE, 5 mV $s^{-1}$, 3 cycles) and electrochemical impedance spectroscopy (EIS) (–0.4 V vs. RHE, amplitude 10 mV, $10^{-1}$～ $10^5$ Hz) were performed to evaluate the HER activity. The electrode surface was observed by SEM-EDX to determine the Mg/Ni ratio of the fabricated Ni plates, and the contact angle $\theta$ was determined by taking a photograph of the electrode surface with 0.1 mL of pure water dropped on the surface.

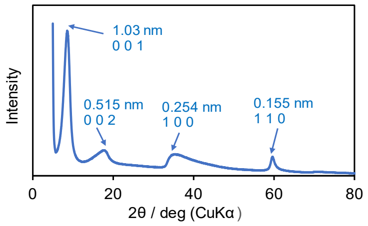

Figure 1 XRD pattern of Mg-ns

## RESULTS AND DISCUSSION

Figure 1 shows that Mg-ns was successfully synthesized like the previous report [5]. The nanosheets observed by AFM are shown in the Figure 2**.** The hexagonal shape with the thickness of about 1 nm and the width of about 400 nm was observed.

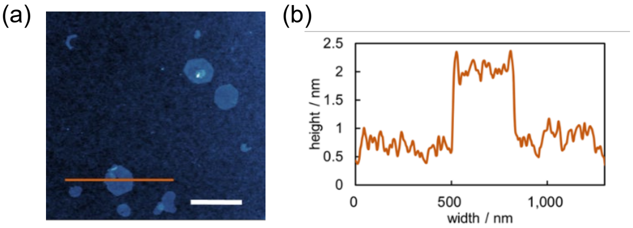

Figure 2 (a) AFM image of the spin-coated Mg-ns. (b) Hight profile on the dashed line indicated in (a)

SEM-EDX showed that the Mg/Ni ratio of the surface of the working electrode increased with the number of spin-coating processes (x5, x10, x20, x30, x50) (Figure 3). The contact angle value ($\theta$) decreased with the plasma treatment and the subsequent spin-coating processes. The change in the contact angle depended on the number of spin-coating processes. The improved wettability is probably due to the hydrophilicity of Mg-ns (Figure 4).Electrochemical measurements on the Tafel gradient showed that the smaller the contact angle θ, the more out of the Tafel region, and the higher the current density side. This suggests that improved wettability may have improved mass transportThe $|i_{\mathrm{real}}|$ at $E$ = –0.5 V vs. RHE was used as an electrode performance affected by mass transport. More wettable electrode exhibited higher $|i_{\mathrm{real}}|$, where Ni plate spin-coated with Mg-ns 50 times and the etched Ni plate exhibited 75.0 and 52.6 mA cm$^{-2}$, respectively. Therefore, the improved wettability due to the Mg-ns coating contributes to the improved HER performance.

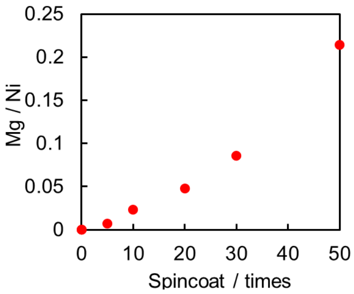

Figure 3 Mg/Ni ratio as a function of the number of spin-coating processes.

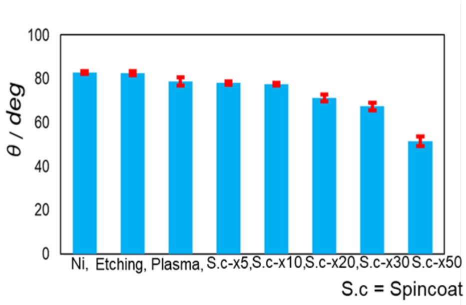

Figure 4 Contact angle of the electrodes.

## CONCLUSION

Partial coating of the electrode surface with Mg-ns improved the wettability of the electrode surface with water and increased HER performance. The improved wettability of the electrode surface may contribute to the higher performance of the cathode, as the bubble is more likely removed from the surface.

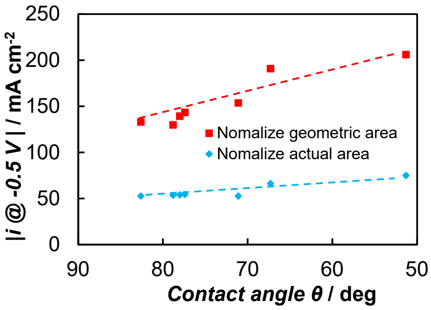

Figure 5 $i_{\mathrm{real}}$ at E = –0.5 V vs. RHE as a function of $\theta$

## REFERENCES

[1] M. Gong *et al.*, *Nano Res.*, **2016**, *9*, 28.
[2] W. Peican *et al.*, *ACS Sust. Chem. Eng.*, **2020**, *8*, 8949.
[3] A. J. Bard, R. Parsons, J. Jordan, Eds., Standard Potentials in Aqueous Solution, Marcel Dekker., 1985.
[4] S. Matsui, I. Tari, *Electrochemistry*, **2003**,*1*,19.

[5] K. Muramatsu *et al.*, *Dalton Trans.*, **2021**, *50*, 3121.

# PREPARATION OF NANOPARTICURATE CATALYSTS FOR POLYMER ELECTROLYTE FUEL CELL CATHODE USING ZR-BASED CLUSTER AS PRECURSOR

Kohei Serizawa[1], Shigenori Mitsushima[1,2], Akimitsu Ishihara[2], Yoshiyuki Kuroda[1,2]
[1]Grad. School of Eng. Sci., Yokohama Natl. Univ., Japan, cel@ynu.ac.jp
[2]Inst. of Adv. Sci., Yokohama Natl. Univ., Japan.

**Keywords:** zirconia, oxygen reduction reaction, graphene, carbon nanotube, cluster precursor, aqueous phase synthesis

## INTRODUCTION

Oxides of group 4 and 5 metals are promising as alternatives of platinum catalysts for oxygen reduction reaction (ORR) catalysts in the cathode of polymer electrolyte fuel cells (PEFCs). Although they are inexpensive and abundant in resources, and high activity has been predicted from DFT caluculations[1], their activity is limited bacause of the low conductivity[2]. Carbon-supported $ZrO_x$ nanoparticle catalysts by pyrolysis and arc plasma deposition have been studied whereas the carbon that serves as the conductive path is easily oxidized and deteriorated in pyrolysis, and it is difficult to uniformly support the arc plasma vapor deposition. In this study, we investigated the homogeneous deposition of $ZrO_x$ nanoparticles by electrostatic immobilization of cationic $Zr_4(OH)_8(H_2O)_{16}Cl_6^{2+}$ clusters (Zr-based clusters) on a graphene oxide (GO) with $-O^-$and $-COO^-$ on the surface, followed by heat treatment to convert the clusters into $ZrO_x$.

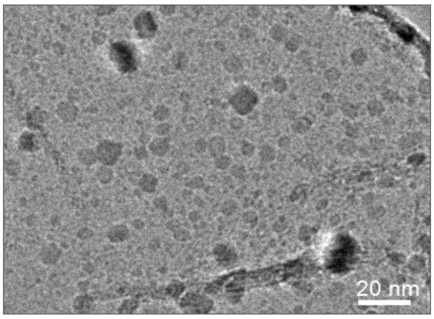
Fig. 1 TEM image of 1000 °C Ar

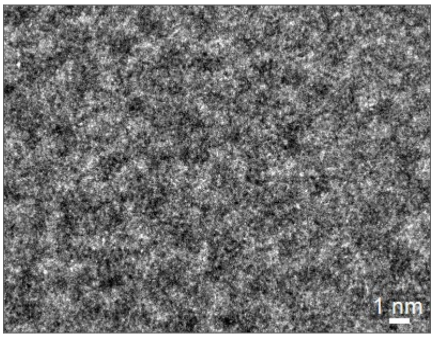
Fig. 2 TEM image of 480 °C Ar

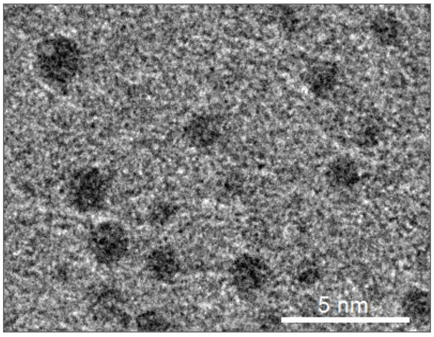
Fig. 3 TEM image of 250 °C $H_2$

## EXPERIMENTAL PROCEDURE

GO and N-doped carbon nanotubes (N-CNT) were dispersed in water, and an aqueous solution of $ZrOCl_2$/HCl at pH 1.4 was added. After stirring at 24 h while forming a Zr-based cluster by hydrolysis, the solids were recovered by filtration. N-CNT was added to prevent surface area reduction due to GO stack. The surface functional group of GO was quantified from acid-base titration, and the amount of each component was determined so that Zr:functional group = 10:1. The obtained composites were reduced under the conditions of 1000 °C Ar, 1h (hereinafter referred to as 1000 °C Ar), 480 °C Ar, 10h (hereinafter referred to as 1000 °C Ar), 480 °C Ar, 10h (hereinafter referred to as 480 °C Ar), 250 °C $H_2$, 2h (less than or equal to 250 °C $H_2$) to obtain a catalyst. The amount of $ZrO_x$ in the catalyst was calculated from the weight reduction due to TG-DTA. The catalyst was supported on a glassy carbon rod (GC) by ink coating method and electrochemical measurements were performed in 0.5 M $H_2SO_4$. Pretreatment CV (0.05–1.20 V, 150 mV $s^{-1}$) was performed in a oxygen atmosphere for 650 cycles. Next, SSV (0.05–1.20 V, 5 mV $s^{-1}$) was performed in $N_2$ and $O_2$ for three cycles in total, and the

ORR current $i_{ORR}$ was calculated from the difference in current value ($i_{N2}$- $i_{O2}$).

## EXPERIMENTAL RESULTS AND DISCUSSION

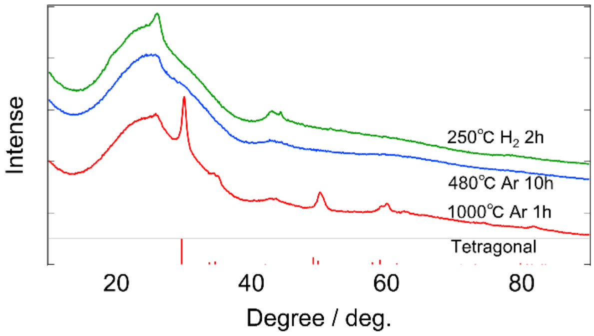

Fig. 4 XRD of each catalyst

From TEM images (Fig. 1-3), it was confirmed that $ZrO_x$ nanoparticles were uniformly supported on GO. $ZrO_x$ nanoparticles were observed in large quantities on a layer of GO, though those on N-CNTs were relatively small. The Zr-based cluster of precursors is probably immobilized on the carbon supports by electrostatic interactions. The amount of acidic functional groups on GO and N-CNTs were 8.49 and 4.85 mmol g$^{-1}$, respectively. Therefore, it is considered that more Zr clusters were supported on GO with a large amount of functional groups. Heat treatment caused clusters to sintering, while the particle size depends on the reduction conditions. Particle sizes were 8.0 nm when heated at 1000 °C in Ar, 1.2 nm when heated at 480 °C in Ar, and 4.0 nm when heated at 250 °C in $H_2$. From the XRD patterns (Fig. 4), $ZrO_x$ in samples treated at 1000 °C Ar was attributed to tetragonal phase $ZrO_2$. Other samples hardly showed peaks. In the sample treated at 480 °C Ar, the disappearance of the peaks should be due to the small particle size. It is thought that amorphous nanoparticles were obtained in samples treated at 250 °C $H_2$. The reaction with $H_2$ may have resulted in a partial reduction of Zr, resulting in rapid agglomeration and inhibition of crystal formation.

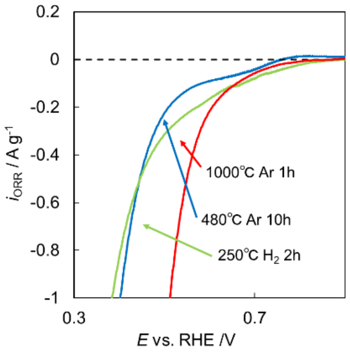

Fig. 5 Polarization curve of each catalyst

From the electrochemical measurements (Fig. 5), the ORR potential at –0.2 A g$^{-1}$ was 0.605 V vs. RHE for the sample heated at 1000 °C in Ar, 0.509 V for that heated at 480 °C in Ar, and 0.571 V for that heated at 250 °C in $H_2$ (In Fig. 5, each polarization curve has a steep slope at –0.2 A g$^{-1}$, so the ORR onset potential is a potential at –0.2 A g$^{-1}$.). Samples heated at 1000 °C in Ar were highly active despite having the largest particle size, and it is thought that highly crystalline nanoparticles are required to use $ZrO_x$ catalysts for ORR.

## CONCLUSION

We succeeded in forming $ZrO_x$ nanoparticles uniformly dispersed on GO by an aqueous solution process using a Zr-based cluster as a precursor. Since ORR activity correlated with crystallinity, a method for preparing highly crystalline microscopic $ZrO_x$ nanoparticles will be studied in the future.

## REFERENCES

[1] Y. Yamamoto, S. Kasamatsu and O. Sugino, J. Phys. Chem. C., Vol. 123 (2019), pp. 19486-19492.

[2] A. Ishihara, T. Nagai, K. Ukita, M. Arao, M. Matsumoto, L. Yu, T. Nakamura, O. Sekizawa, Y. Takagi, K. Matsuzawa, T. W. Napporn, S. Mitsuhima, T. Uruga, T. Yokoyama, Y. Iwasawa, H. Imai and K. Ota, J. Phys. Chem. C., Vol. 123 (2019), pp. 18150-18159.

P15

# Investigation of the Cycling Stability of Room-Temperature Metal Hydrides (MHs)

Dmytro Stepanov, Eveline Kuhnert, Merit Bodner

*Institute of Chemical Engineering and Environmental Technology, Graz University of Technology, Inffeldgasse 25/C, 8010 Graz, Austria, d.stepanov@tugraz.at*

**Keywords:**. Metal hydride, hydrogen storage, cycle stability, accelerated stress cycling.

Metal hydride (MH) hydrogen storage is a highly promising method, especially under room temperature conditions[1]. Compared to other hydrogen storage methods, no significant energy input for heating, cooling, or achieving high pressure is needed [2]. The process of hydrogen sorption in the MH is an exothermic reaction, which involves heat release, and the desorption process is endothermic and heat energy is consumed. For RT MHs this energy is emitted to environment by charging and taken from environment by discharging. Therefore, the reaction rate of these processes depends on the temperature conditions in which the charging- and discharging cycles are carried out. The cyclic stability is one of the most important properties for the evaluation and characterization of MH storage tanks. It is the ability to absorb and release hydrogen over a large number of charge- and discharge cycles without a loss in capacity.

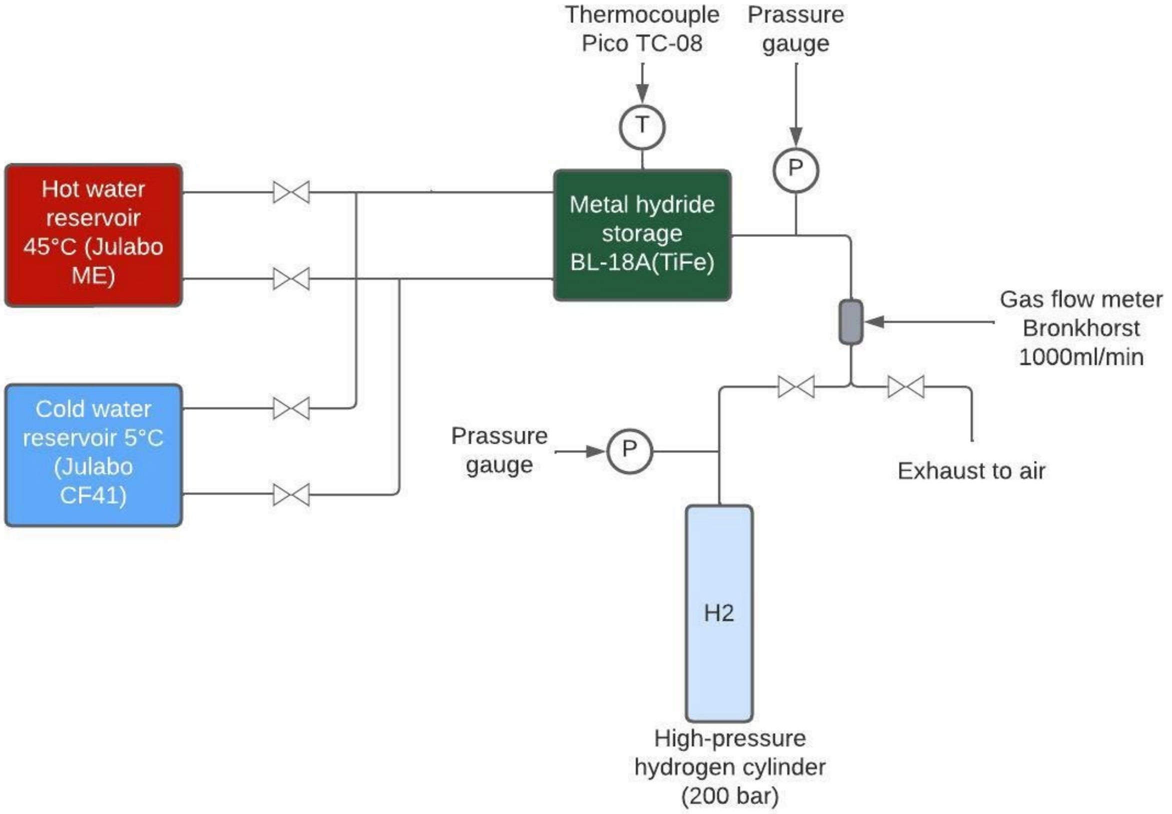

Figure 1. P&ID of the MH Storage Test Rig.

In this work, a method is developed to analyze the cyclic stability of low-temperature MHs. Accelerated stress cycling (ASC) is performed by controlling the charge- and discharge temperature of the MH storage, for this purpose a test rig was set up (Fig.1). The object of the study is a 20 nL TiFe Hydrogen Components, Inc. BL-18 MH storage tank. Thermal parameters of the charging and discharging process are measured by a thermocouple and a thermal imaging camera. The charge- and discharge rate, volumetric values as well as the flow rate (mL/min) are determined by a mass flow meter (max. = 1000 mL/min). The capacity values were additionally determined by gravimetric measurements. The desired temperature range was achieved using water circulators. In the process of experiments, it was found that by controlling and maintaining the targeted temperature range of sorption- and desorption, both the charging and discharging cycles are significantly accelerated. The increase in the flow rate in the first 15-20 minutes of the cycle allows the development of a set of ASC protocols. After the flow rate investigation of temperature-controlled cycles, it was decided to limit the ASCs with a lower flow rate of 100mL/min.

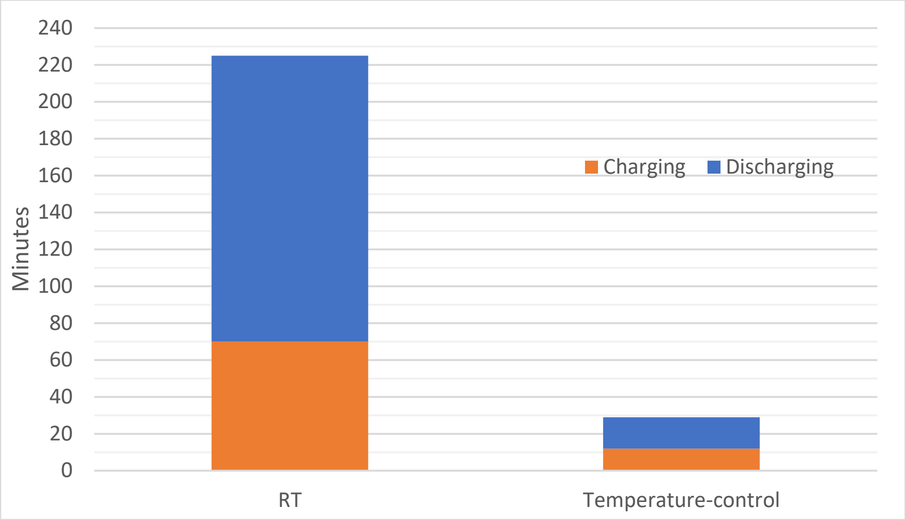

Figure 2. Charge/discharge cycle time comparison RT vs Temperature-control.

By using temperature-control at 100mL/min flow rate, the volume reaches a value of about 80% of full capacity. The usage of temperature-control decreases charging cycle time by 80% and discharging cycle time by 90%. An overall 8-fold decrease of cycle-time could be observed compared to RT.

## ACKNOWLEDGMENT

Financial support by the Austrian Research Promotion Agency (FFG) through the 8th Call of “COMET-Project” is gratefully acknowledged.

## REFERENCES

[1]. Modi Poojan, Aguey-Zinsou Kondo-Francois, Room Temperature Metal Hydrides for Stationary and Heat Storage Applications: A Review, Front. Energy Res., 09 April 2021 Sec. Hydrogen Storage and Production, ISSN=2296-598X, https://doi.org/10.3389/fenrg.2021.616115
[2]. I.A. Hassan, Haitham S. Ramadan, Mohamed A. Saleh, Daniel Hissel, Hydrogen storage technologies for stationary and mobile applications: Review, analysis and perspectives, Renewable and Sustainable Energy Reviews,Volume 149, 2021, 111311, ISSN 1364-0321, https://doi.org/10.1016/j.rser.2021.111311

P16

# UTILIZATION OF RAW BIOGAS FOR HIGH-PURITY HYDROGEN PRODUCTION VIA CHEMICAL LOOPING

STOPPACHER Bernd[1], HACKER Viktor[2]

[1] Institute of Chemical Engineering and Environmental Technology, Graz University of Technology
Inffeldgasse 25C, 8010 Graz, Austria, +43 316 873 4971, bernd.stoppacher@tugraz.at
[2] Institute of Chemical Engineering and Environmental Technology, Graz University of Technology
Inffeldgasse 25C, 8010 Graz, Austria, +43 316 873 8780, viktor.hacker@tugraz.at

**Keywords:** Chemical Looping, Biogas conversion, Decentralized hydrogen production

## ABSTRACT

The utilization of industrial and agricultural waste streams for the production of high-value energy carriers will be pivotal in the transition towards a sustainable energy system. Biogas from the digestion of biogenic residues provides a promising alternative feedstock for decentralized hydrogen production.

The Reformer Steam Iron Cycle (RESC) is a chemical looping-based fixed-bed process for the production of high-purity hydrogen from fossil and biogenic primary energy sources [1]. In the Austrian research project Biogas$_2$H$_2$, a 10 kW$_{th}$ fixed-bed chemical looping laboratory system was coupled to a 3 MW$_{th}$ biogas digester in the southern region of Austria. Thirty redox cycles were performed in an experimental study. The generated hydrogen was characterized online by ppm-range gas analysis and exhibited a product gas quality of up to 99.998%. Throughout a parameter study, the influence of relevant process parameters (temperature, O/R ratio, reduction time, amount of steam in the oxidation phase) on the hydrogen purity and system efficiency was observed [2].

In general, the utilization of biogenic gases implicates the introduction of harmful sulfur contaminants in the process. Previous investigations in laboratory scale showed that hydrogen sulfide in the feed gas causes significant contamination of the product hydrogen and a performance loss of 12% in case of 100 ppm in the reductive feed gas. The reason was found in molecular chemisorption of $H_2S$ on the surface of the oxygen carrier throughout the reduction phase. In the subsequent steam oxidation phase hydrogen sulfide desorbs again and enters the product gas stream [3].

The results of the project Bioga$_2$H$_2$ proofed that coupling fixed-bed chemical looping systems to biogas plants enable a fuel cell grade hydrogen qualitiy and an economically competitive option for upgrading local available biogenic residuals to high-purity hydrogen [4].

## ACKNOWLEDGEMENTS

Financial support from the Austrian Research Promotion Agency through the 30th Bridge Call is gratefully acknowledged.

## REFERENCES

[1] V. Hacker, “A novel process for stationary hydrogen production: the reformer sponge iron cycle (RESC),” *J. Power Sources*, vol. 118, pp. 311–314, 2003.

[2] B. Stoppacher, T. Sterniczky, S. Bock, and V. Hacker, “On-site production of high-purity hydrogen from raw biogas with fixed-bed chemical looping,” *Energy Convers. Manag.*, 2022.

[3] B. Stoppacher, S. Bock, K. Malli, M. Lammer, and V. Hacker, “The influence of hydrogen sulfide contaminations on hydrogen production in chemical looping processes,” *Fuel*, vol. 307, no. August 2021, p. 121677, 2022, doi: 10.1016/j.fuel.2021.121677.

[4] S. Bock, B. Stoppacher, K. Malli, M. Lammer, and V. Hacker, “Techno-economic analysis of fixed-bed chemical looping for decentralized, fuel-cell-grade hydrogen production coupled with a 3 MWth biogas digester,” *Energy Convers. Manag.*, vol. 250, no. September, p. 114801, 2021, doi: 10.1016/j.enconman.2021.114801.

P17

# Performance Analysis of Protonic Ceramic Fuel Cell Cogeneration System using Methane Fuel

F. Suito[1], K. Li[1], Y. Nagata[1], T. Murakami[1], T. Araki[1]

[1] Yokohama National University, 79-5 Tokiwadai, Hodogaya, Yokohama, Kanagawa 240-8501, Japan

**Keywords:**. Protonic ceramic fuel cells (PCFCs), Residential cogeneration system, Methane, Reforming

In recent years, there has been growing interest in developing protonic ceramic fuel cells (PCFCs) with proton conductive electrolyte. One of these reasons is that PCFCs have a possibility of higher generation efficiency than that of solid oxide fuel cells (SOFCs) with oxide-ion conductive electrolyte, due to less fuel dilution at fuel electrode side using $H_2$ fuel.

However, the supply chain of hydrogen would be not established for a while. On the other hand, the city gas, which is composed mainly of methane, has been installed, especially in large cities. When energy efficiency of PCFC system is higher than that of SOFC one using methane as fuel, it can be applied to a wide variety of power generators and cogeneration systems. In the present paper, the

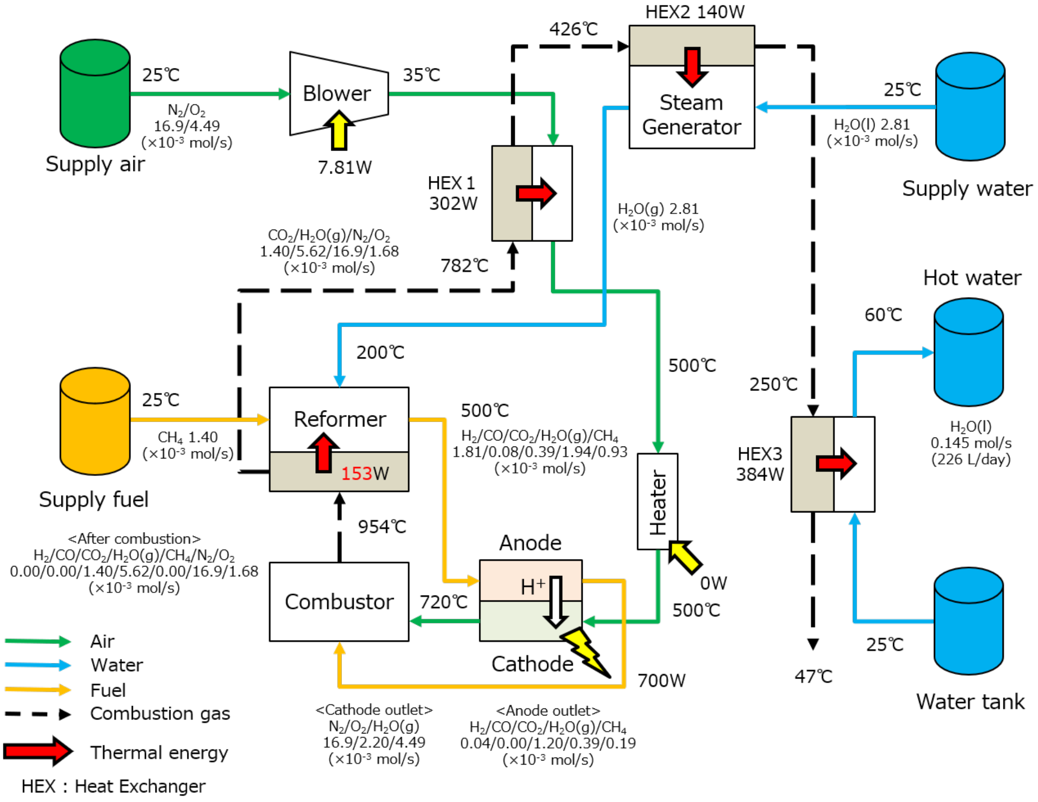

Fig. 1 Process flow diagram of an PCFC cogeneration system using methane as fuel

performance of the PCFC residential cogeneration system is compared to that of the system with SOFC, when methane fuel is used.

As shown in Fig. 1, we assume a simple model of PCFC residential cogeneration system that consists of an air-blower, a reformer, a combustor and four heat-exchangers. The calculation of energy efficiency in this system is carried out using several parameters, such as cell voltage, operating temperature, and fuel utilization. Table 1 shows the standard conditions for the system calculation and Table 2 shows the results. The more detailed results will be discussed in the presentation.

Table 1 Standard conditions for calculation

| **Parameters** | **Value** | **Unit** |
|---|---|---|
| S/C | 2 | [-] |
| Supply $CH_4$ | $1.40 \times 10^{-3}$ | [mol/s] |
| Supply $H_2O(l)$ | $2.81 \times 10^{-3}$ | [mol/s] |
| Supply $O_2$ | $4.49 \times 10^{-3}$ | [mol/s] |
| Supply $N_2$ | $1.69 \times 10^{-2}$ | [mol/s] |
| Operating temperature | 873.15 | [K] |
| Cell voltage | 0.85 | [V] |
| Fuel utilization | 80 | [%] |
| Air utilization | 50 | [%] |
| Inverter efficiency | 95 | [%] |
| Current efficiency | 100 | [%] |
| Heat loss at heat exchangers | 5 | [%] |
| Heat loss at PCFC | 10 | [%] |
| Heat loss at combustor | 10 | [%] |

Table 2 Results of calculation under standard conditions

| **Efficiency** | **Value** | **Unit** |
|---|---|---|
| Power generation efficiency (LHV) | 61.69 | [%] |
| Heat recovery efficiency | 38.06 | [%] |
| Total efficiency | 99.76 | [%] |

P18

# EFFECTS OF SURFACE TEXTURE FOR VAPOR CONDENSATION WITH NON-CONDENSABLE GAS

SUZUKI Daichi[1], ARAKI Takuto[2]

[1]Grad. Sch. of Eng. Sci., Yokohama National Univ., Tokiwadai 79-5, Hodogaya-ku, Yokohama, Kanagawa pref., Japan, suzuki-daichi-zw@ynu.jp

[2] Faculty of Eng., Yokohama National Univ., Tokiwadai 79-5, Hodogaya-ku, Yokohama, Kanagawa pref., Japan

**Keywords:** Vapor condensation, Non-condensable gas.

## INTRODUCTION

Condensation of water vapor in non-condensable gas (NCG) is a familiar phenomenon. This phenomenon occurs in many industrial situations, such as seawater desalination and metal corrosion in structures[1,2]. In pure water vapor or vapor in a low NCG fraction, the condensation rate is mainly governed by condensation morphologies due to the wettability of condensation surfaces in the same temperature fields[3]. However, when investigating steam condensation in the high NCG fraction, it is necessary to consider the mass transport of vapor. Therefore, vapor condensation in the high NCG fraction is considered a more complex phenomenon than condensation in the low NCG fraction. This study focuses on water vapor condensation in high NCG fraction conditions. In this study, we proposed a method for measuring water vapor condensation in the high NCG fraction by measuring the weight increase of condensation droplets (hereinafter referred to as the gravimetric method). Existing studies have used the method of measuring the condensation rate by measuring the temperature gradient near the condensation surface and deriving its heat flux, or by measuring the area occupancy of condensation droplets on the condensation surface[4]. The condensation rate in high NCG fractions, which is the subject of this study, is smaller than that in pure steam, and the temperature change is considered to be relatively small. Therefore, it is difficult to measure the condensation rate by the method that derives the condensation rate from the temperature change. In addition, the image processing lacks quantitative in consideration of the contact angle of droplets. Therefore, we proposed and employed the gravimetric method, which enables quantitative measurement in high NCG fractions, and conducted experiments.

## EXPERIMENTAL

Figure 1 shows a schematic diagram of the experimental apparatus and condensing section. A 2 mm-thick Al plate was attached to the heat-absorbing surface of the Peltier element to serve as the condensing surface, and a heat sink was attached to the heat-dissipating surface to promote heat dissipation by using a blower to blow air. A K-type thermocouple was inserted on the underside of the Al plate to measure the condensing surface temperature. urethane foam was applied to the Peltier element and the sides of the Al plate to prevent condensation from occurring outside the Al surface and causing measurement errors. In the condensation generation section, a channel made of acrylic ABS resin was installed to cover the Al surface, which is the condensation surface, and an experimental atmosphere was set up by flowing a supply gas through the channel. The channel structures are shown in Figure 1. These were placed on an electronic balance (Shimadzu APX-324X) and the weight of the condensate was measured.

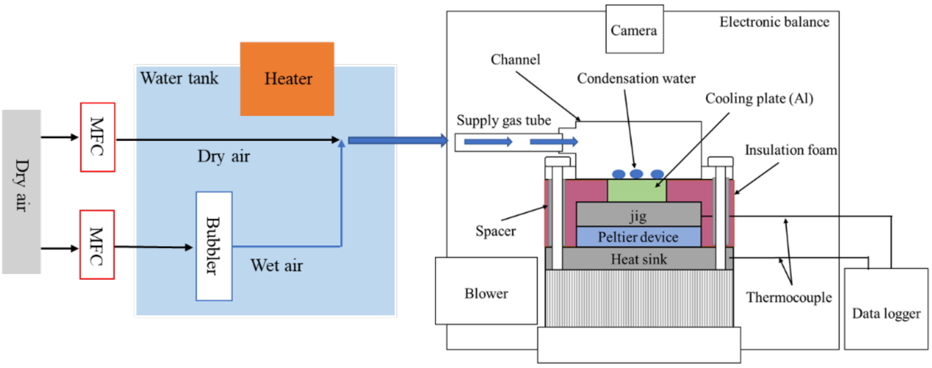

Gas supply system

Test section

Fig.1 Experimental apparatus

## RESULTS AND DISCUSSION

To validate the experimental setup, the condensation rate on a flat Al plate(2mm thickness) at Re88 was measured. Results are shown in Figure 2. Measured weights increased linearly with time at RH15/20, and at RH0, measured weights were within ±0.003g in 30 minutes, suggesting that the measurement was valid.

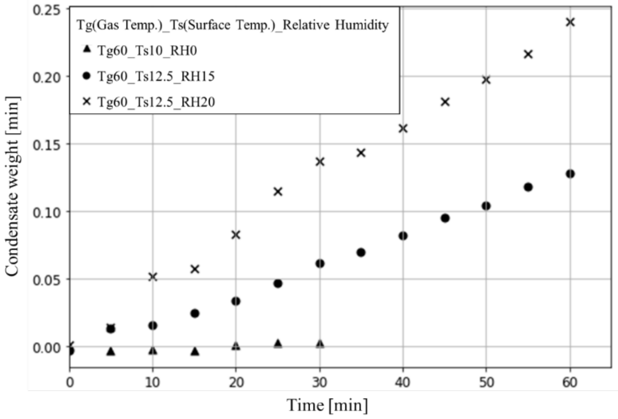

Fig.2 Variation of condensation on Al surface

## CONCLUSION

An experimental apparatus to quantitatively measure water vapor condensation was developed. Using this device, we will conduct experiments with materials and conditions such as condensation inside porous materials like GDL, which cannot be measured by existing measurement methods.

## REFERENCES

[1] V. G Rifert et al. Desalination, vol. 74(1989), pp.373-382
[2] S. Zhang et al. Colloids and Surface A, vol. 585(2020), pp.1-8
[3] B. Chung et al. Int. Comm. Heat Mass Transfer, Vol. 31(2004), No. 8, pp. 1067-1074
[4] N. S. Singh et al. Adv. Mater. Interfaces, Vol. 8(2021), pp.2001442-200170

P19

# NUMERICAL ANALYSIS OF DEPENDENCE OF LEAKAGE CURRENT ON GAS PARTIAL PRESSURES IN PCFC

Ryogo Takatera[1], Kunpeng Li[2], Takuto Araki[3]

[1]Graduate School of Engineering, Yokohama National University, Kanagawa, 240-8501, Japan, takatera-ryogo-dx@ynu.jp,
[2]Graduate School of Engineering Science, Yokohama National University, Kanagawa, 240-8501, Japan, li-kunpeng-vk@ynu.ac.jp
[3]Faculty of Engineering, Yokohama National University, Kanagawa, 240-8501, Japan, taraki@ynu.ac.jp.

**Keywords:**. Proton ceramic fuel cell(PCFC), Nernst-Planck-Poisson (NPP) mode, gas partial pressures.

## INTRODUCTION

Proton-conducting ceramic fuel cells (PCFCs) have attracted attention as a highly efficient energy conversion device. The electrolyte in PCFCs exhibits high proton conductivity at relatively low temperatures, but also exhibits hole conductivity under certain conditions. This hole migration is regarded as a leakage current and leads to a decrease in current efficiency or power generation efficiency. The proton and hole conductivities are greatly affected by the gas atmosphere, such as water vapor and oxygen partial pressures, and the local temperature, but the effect of the gas concentration distribution on the local current distribution inside the cell is complex. Therefore, a two-dimensional Nernst-Planck-Poisson (NPP) model was used to numerically analyze the effect of the gas atmosphere distribution on the cell performance. Figure 1 shows the governing equations at the PCFC electrolyte interface and inside.

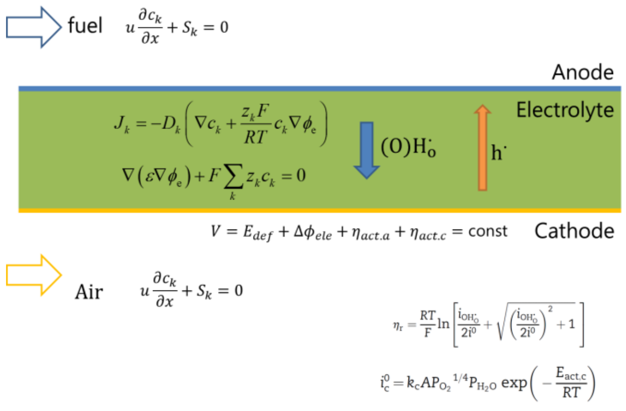

Fig. 1 Governing equations inside and at the interface of the electrolyte in PCFC

The analytical conditions were assumed to be counter-current flow with 3% humidified pure hydrogen fuel supplied to the anode of an 8um-thick electrolyte and air supplied to the cathode. Hydrogen and oxygen utilization were set to 90% and 30%, respectively, and the reference cell voltage was set to 0.7V.

## RESULT

Figures 2 and 3 show the distribution of hole and proton concentrations in the electrolyte at 600°C, respectively. The front side of each figure shows the gas inlet, the back side shows the gas outlet, the lower right side shows the anode, and the upper left side shows the cathode.

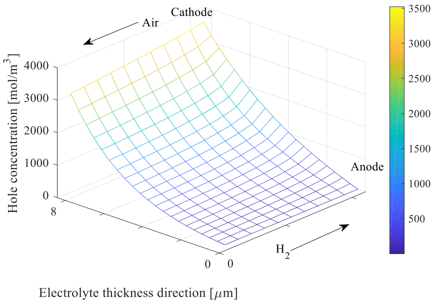

Fig.2 Hole concentration distributions (600℃)

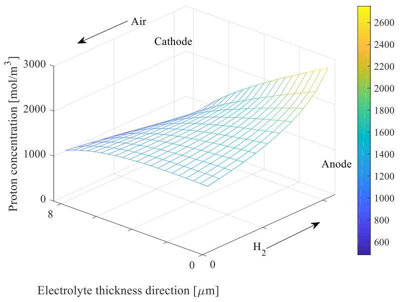

Fig.3 Proton concentration distributions (600℃)

Figure 2 shows that the hole concentration on the cathode side is higher than that on the anode side. This corresponds mainly to the higher oxygen concentration at the cathode. On the cathode side, the oxygen concentration decreases as oxygen is consumed by the power generation reaction downstream and water vapor is generated. Therefore, the hole concentration also decreases slightly.

The proton distribution in Figure 3 shows that the proton concentration increases downstream of both the cathode and anode. This is because water vapor is generated by the electrochemical reaction at the cathode, resulting in an increase in water vapor concentration, and hydrogen is consumed by the power generation reaction at the anode, resulting in a relative increase in water vapor concentration, resulting in an increase in proton concentration downstream. It should be noted, however, that the absolute value of the proton concentration contains uncertainty due to insufficient experimental data on hydration equilibrium.

## ACKNOWLEDGMENTS

Part of these results were obtained as a result of the New Energy and Industrial Technology Development Organization (NEDO) commissioned research and development of ultra-high efficiency proton-conducting ceramic fuel cell devices (JPNP20003).

## REFERENCES

[1] K. Li et al., Int. J. Hydrogen Energy, Vol. 45 (58), Page 34139-34149, (2020)
[2] Y. Okuyama, et al., J. Hydrogen Energy 39 (2014) 20829-36.

# EVALUATION METHOD FOR ELECTROCATALYST ACTIVITY FOR GAS EVOLUTION REACTION

Yu Takenaga,[1] Kunpeng Li,[2] Kensaku Nagasawa,[2] Yoshiyuki Kuroda,[1,2] and Shigenori Mitsushima[1,2]

[1]*Graduate School of Engineering Science, Yokohama National University, 79-5 Tokiwadai, Hodogaya-ku, Yokohama 240-8501, Japan*
[2]*Institute of Advanced Sciences, Yokohama National University, 79-5 Tokiwadai, Hodogaya-ku, Yokohama 240-8501, Japan*
E-mail: ynugr-cel@ynu.ac.jp

**Keywords:** Powder electrocatalyst, Alkaline water electrolysis, Oxygen evolution reaction

## INTRODUCTION

To determine the oxygen evolution reaction (OER) activity of powder catalysts, the three-electrode cell with a rotating disk electrode (RDE) is usually employed, which is based on electrochemical method for fuel cell catalysts. However, even with basic electrolytes, Nafion is used as a binder, and oxygen bubbles inhibit mass transfer and catalyst desorption. For this reason, small size electrolyzer is usually applied for durability evaluation of catalysts [1].

In this study, to develop an electrochemical method to evaluate the activity of powder catalysts without binder for gas evolution reaction in a practical high current density range, we have analyzed transition current of chronoamperometry (CA) to get oxygen bubble free current using forced flow cell that fastens powder electrocatalysts.

## EXPERIMENTAL

1 cm$^2$ electrolyzer with an independent effective area contact control system was used. Figure 1 shows a schematic diagram of the catalyst fastening section of that electrolyzer. A catalyst was fastened between a diaphragm membrane and a rib of the current corrector, and electrolyte flowed through catalyst layer in interdigit forced flow field.

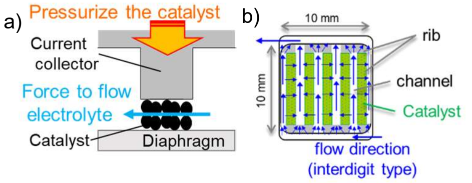

Fig. 1. Schematic drawing of the electrolyzer structure: a) place of catalyst and flow of electrolyte, b) catalyst attached area.

KCl saturated Ag/AgCl references were placed on the membrane by the contact with 7 M KOH, and potential was indicated based on reversible hydrogen electrode. The anode current collector is made of Pt-plated Ti. The anode and the cathode electrocatalyst are$LaNiO_3$ (LNO, 98.5 wt%, particle size 104 nm, 80.1 mg$_{\text{-LNO}}$/cm$^2$, self-made by sol-gel method), and Pt/C (TKK). The anode catalyst was coated with the shape of the rib of 1 mm width rectangular array onto Zirfon membrane, and the cathode catalyst was coated onto a carbon paper (39BC, SGL) as cathode electrode. The loading amount of catalyst was analyzed by XRF before electrochemical measurements.

The temperature was 30℃ and the electrolyte was 7 M KOH, circulating at 100 and 30 mL min$^{-1}$ in the working and counter electrode chambers. After chronopotentiometry (CP) at 1 A cm$^{-2}$ as a pretreatment, electrochemical measurements were made at CA. OER was evaluated by potential step from 1.50 V for 360 s of potential hold to the measured potential in the rage from1.51 to 1.90 V for 10 s. The electrochemical impedance spectroscopy (EIS) was performed to evaluate internal resistance.

The current in CA decays with time. If the current decay is dominated by diffusion according to the Cottrell equation, inverse of current is linear relation to squire root of time with intercept of inverse of kinetic current

$$1/i = 1/i_k + 1/i_d = 1/i_k + (\pi t)^{1/2}/\left(nFCD^{\frac{1}{2}}\right) \qquad (1)$$

where $i_k$ : kinetic current density, $i_d$ : diffusion-limited current density, $F$ : Faraday constant, $C$: substrate concentration, $D$: diffusion coefficient. All except time $t$ in the second term could be treated as constants. Therefore, the inverse of the measured current is linear to the square root of time, and the inverse of kinetic current is obtained from time zero extrapolated the inverse of the measured current as a function of square root of time [2, 3].

## RESULTS AND DISCUSSION

Figure 2 shows the plots of the square root of time versus the relative of the reciprocal current density with 100 ms as the reference. If the current decrease like as Cottrell equation, the current shows linear region later than the completion of charging of the electric double layer of a few ms, but clear linear region was not observed at any potential. At the initial period of current decrease would be affected by supersaturation near the catalyst, and the second region would be affected by bubbles formation, which follows the same analogy as diffusion and follows equation (1). After the second region, the current becomes steady state [3].

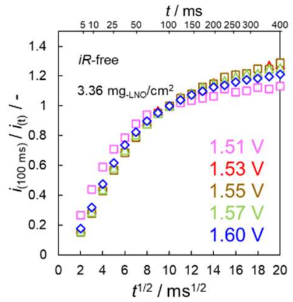

Fig. 2. The relative reciprocal current density as a fanction of the square root of time for CA.

To find the second region, the second-order derivative of Fig. 2 is shown in Fig. 3. A negative peak of the second-order derivative was observed for each potential, and the time domain of the peak was treated as the Cottrell equation like behavior. The kinetic current density was determined by extrapolating time zero from Fig. 2.

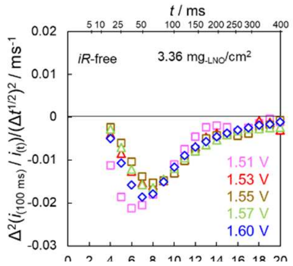

Fig. 3. The negative peak of the second-order derivative of the relative reciprocal current density per step potential.

Figure 4 shows the obtained polarization curves normalized the BET surface area of the LNO for various catalyst loadings. No significant dependence of $i_{\text{specific}}$ on the loading was observed and the Tafel slope was in the range from 57 to 68 mV/dec for 1.51 to 1.60 V, which is almost same as 40 to 100 mV/dec obtained by the ink application method with RDE [4, 5]. The evaluation range of current density in the conventional RDE method is 0.01 to 0.1 mA $cm^{-2}{}_{\text{-BET}}$ at 1.6 V [5]. On the other hand, this time zero analysis method reaches the same current density at 1.52 to 1.57 V. This would indicate that the suppression of OER activity by bubbles could be eliminated even it is difficult to evaluate the influence of generated gas bubbles to mass transfer or detachment of the catalyst, which makes difficulty to apply to durability evaluation using RDE [1]. Furthermore, the proposed method using time zero analysis overcomes gas stagnation or catalyst detachment, and is expected to be applied to durability evaluation with accelerated durability test (ADT) [6].

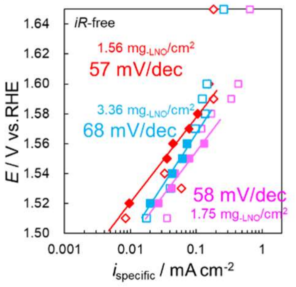

Fig. 4. Specific activity of $LaNiO_3$ based on BET surface area.

## ACKNOWLEDGEMENTS

This study was based on results obtained from the Development of Fundamental Technology for Advancement of Water Electrolysis Hydrogen Production in Advancement of Hydrogen Technologies and Utilization Project (JPNP14021) commissioned by the New Energy and Industrial Technology Development Organization (NEDO) in Japan.

## REFERENCES

[1] H. A. El-Sayed, et al., *J. Electrochem. Soc.*, **166**, (8), 458-464, (2019).

[2] K. Nagasawa, I. Matsuura, Y. Kuroda, S. Mitsushima, *Electrochemistry*, **90**, 017012, (2022).

[3] K. Nagasawa, L. Kunpeng, Y. Takenaga, Y. Kuroda, S. Mitsushima, *Electrochemistry*, **90**, 047004, (2022).

[4] Y. Tsukada, Y. Kuroda, H. Niiro, Y. Fujii, N. Fujimoto, S. Mitsushima, *Electrochim. Acta.*, **353**, 136544, (2020).

[5] S. Jung, C. C. L. McCrory, I. M. Ferrer, J. C. Peters, T. F. Jaramillo, *J. Mater. Chem. A*, **4**, 3068-3076, (2016).

[6] A. Abdel Haleem, K. Nagasawa, Y. Kuroda, Y. Nishiki, A. Zaenal, S. Mitsushima, *Electrochemistry*, **89**, 186-191, (2021).

P21

# COATINGS FOR ADVANCED FUNCTIONALIZED GAS DIFFUSION LAYERS IN FUEL CELLS

TRITSCHER Florian and BODNER Merit

Institute for Chemical Engineering and Environmental Technology, Inffeldgasse 25/C, A-8010 Graz, tritscher@tugraz.at

**Keywords:**. fuel cell, gas diffusion layer, polymers, coatings, electrochemical polymerization, dip coating, carbon paper

Gas diffusion layers (GDLs) are an essential part of polymer electrolyte fuel cells (PEFCs), responsible for mass transport, water management and the conduction of electrons. For these purposes, the materials which make up the GDL need to possess certain attributes such as electrical conductivity, suitable wettability, porosity and (electro)chemical stability in the environment of a PEFC [1]. Nowadays, state of the art GDLs consist of a carbon paper called macroporous substrate (MPS) and an additional microporous layer (MPL). Despite being carbon based, GDLs are fabricated from petroleum based polyacrylonitrile (PAN) and the production of low cost, durable and environmentally friendly GDLs is still a challenge [2].

Although PAN as starting material is low in price, it needs to be processed to obtain the required porosity and conductivity. During the processing steps, high temperatures are needed to convert the material via pyrolysis into carbon paper. Furthermore, the addition of polytetrafluoroethylene (PTFE) to improve the hydrophobic properties as well as the application of the MPL increase the cost of the material [2]. Moreover, the addition of PTFE limits the feasibility of recycling of the material due to the introduction of fluorine containing compounds. Another challenge is durability since these materials are prone to oxidation, leading to a loss of their properties and contributing to the aging of the fuel cell [3].

Due to the environmental concerns, there are some researchers focused on developing new kinds of GDLs based on renewable resources such as cotton and jute [2,4]. However, these materials show poor stability and water transport properties. The aim of this work is to provide a solution to these challenges via developing functional coatings for GDLs.

Coatings consisting of conducting polymers (eg. polyaniline (PANI), polypyrrole (PPy)) or reduced graphene oxide (rGO) promise to advance the material development due to electrical conductivity, adaptable wettability and electrochemical stability. In addition, conducting polymers have been implemented as anti-corrosion coating for steel [5]. For coating the carbon papers with a polymer, methods such as electrochemical polymerization (see Fig. 1) or dip coating in combination with chemical oxidative polymerization have already been investigated for supercapacitor applications [6]. However, due to the distinct requirements for fuel cells, these methods need to be adapted for successful implementation.

The possibility of adapting the properties of the polymer coating is manifold and one of the main challenges of this work. The chain length, morphology, incorporation of dopants and additives as well as the coating technique all influence the properties of the resulting coating [7]. Therefore, this work contains the identification of possible coatings and coating techniques for gas diffusion layers and the (electro)chemical, optical and mechanical characterisation, followed by in-situ testing of the new GDL in a fuel cell.

Conclusively, the development of a functional coating for gas diffusion layers promises to advance the substitution of petroleum-based materials with renewable resources and reduce production cost by avoiding expensive processing steps.

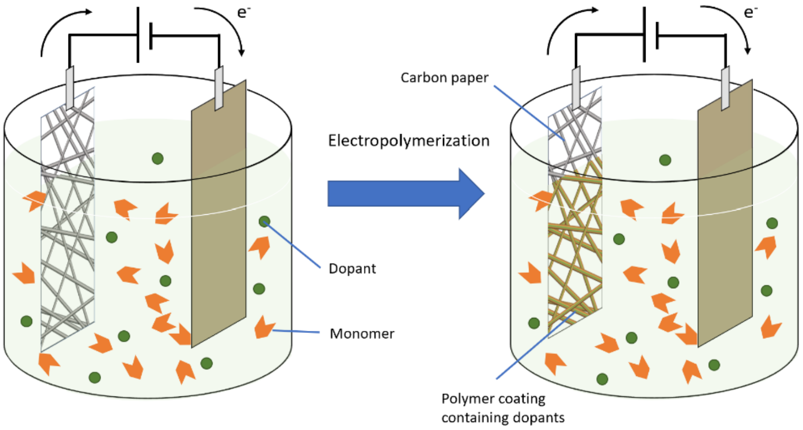

Fig. 1: Electropolymerization as coating technique for functionalized carbon paper

## ACKNOWLEDGEMENT

This work was funded by the Anschubsfinanzierung of the Field of Expertise “Mobility and Production” of the Graz University of Technology.

## REFERENCES

[1] A. Ozden, S. Shahgaldi, X. Li, and F. Hamdullahpur, Progress in Energy and Combustion Science, vol. 74. Elsevier Ltd, pp. 50–102, Sep. 01, 2019.

[2] D. P. Leonard and R. L. Borup, ECS Meeting Abstracts, vol. MA2019-02, no. 32, pp. 1426–1426, Sep. 2019.

[3] I. Jiménez-Morales et al., Carbon Energy, vol. 3, no. 4, pp. 654–665, Aug. 2021.

[4] A. Navarro, M. Gómez, L. Daza and J.J. Lopez-Cascales, Research Square, Oct. 2022.

[5] A. Adhikari et al., High Performance Polymers, vol. 30, no. 2, pp. 181–191, Mar. 2018.

[6] J. Xing, M. Liao, C. Zhang, M. Yin, D. Li, and Y. Song, Physical Chemistry Chemical Physics, vol. 19, no. 21, pp. 14030–14041, 2017.

[7] T. Darmanin and F. Guittard, Progress in Polymer Science, vol. 39, no. 4. Elsevier Ltd, pp. 656–682, 2014.

P22

# INVESTIGATION OF DISSOLVED OXYGEN FIELD BY VISUALIZING OXYGEN BUBBLES NEAR ANODE CATALYST ELECTRODE IN PEM WATER ELECTROLYZER

Kohei Wakudar[1], Konosuke Watanabe[2], Hideki Suwa[3], Ryo Kanemoto[3], Takuto Araki[3], Kensaku Nagasawa[4] and Shigenori Mitsushima[4]

[1]YNU Interfaculty Graduate School, Yokohama National University, Kanagawa, Japan, wakuda-kohei-by@ynu.jp
[2]Department of Mechanical Engineering, National Institute of Advanced Industrial Science and Technology, Nagoya, Japan,
[3]Department of Mechanical Engineering, Yokohama National University, Kanagawa, Japan,
[4]Department of chemical Engineering, Yokohama National University, Kanagawa, Japan,

**Keywords:**. PEMWE, Dissolved oxygen, Mass transport loss, Oxygen supersaturated region, Visualising observation

## 1.INTRODUCTION

In order to expand the practical application range of the proton exchange membrane water electrolyzers (PEMWE), it is necessary to reduce the mass transport loss due to oxygen at the anode. Oxygen transport near the catalyst layer (CL) is thought to have two transport mechanisms, gaseous oxygen and dissolved oxygen. However, as far as we know, there are no reports of experimental investigation of the presence of dissolved oxygen in PEMWE. In this study, the behavior of bubbles floating near CL was observed with a high-speed camera, and the bubble diameter was measured. Even after the bubbles left the CL surface, the bubble diameter continued to increase, confirming the presence of dissolved oxygen and the formation of an oxygen supersaturated region.

## 2.EXPERERIMENTAL

Fig.1 shows the appearance of the PEMWE visualization cell used in this study. A transparent acrylic plate was placed on the side of the cell, and oxygen bubbles generated at the PTL-CL interface were filmed by a high-speed camera through the acrylic plate. The bubble diameter was measured by specifying three points on the outline of the bubble in the video.

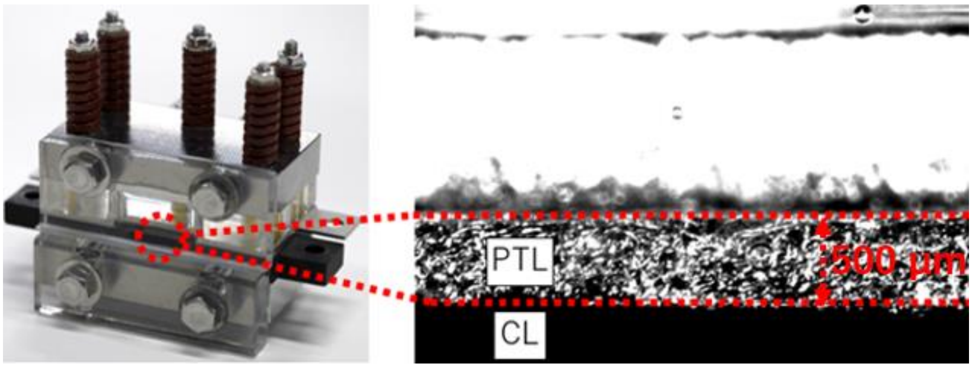

Fig.1 Appearance of the cell and shooting

## 3.RESULT

### 3-1. Floating oxygen bubbles

In the video taken, various bubble behaviors were observed, including those that coalesced on the anode CL surface after generation, those that detached from the anode CL surface and floated, those that adhered to the sides of the anode PTL, and those that coalesced on the sides. The electrolysis conditions were constant current operation at 100 mA/cm$^2$. The growth behavior of bubbles was evaluated by measuring their diameters. Fig.2 shows the relationship between the measured bubble diameters and the distance between the bubbles and the anode CL surface during levitation.

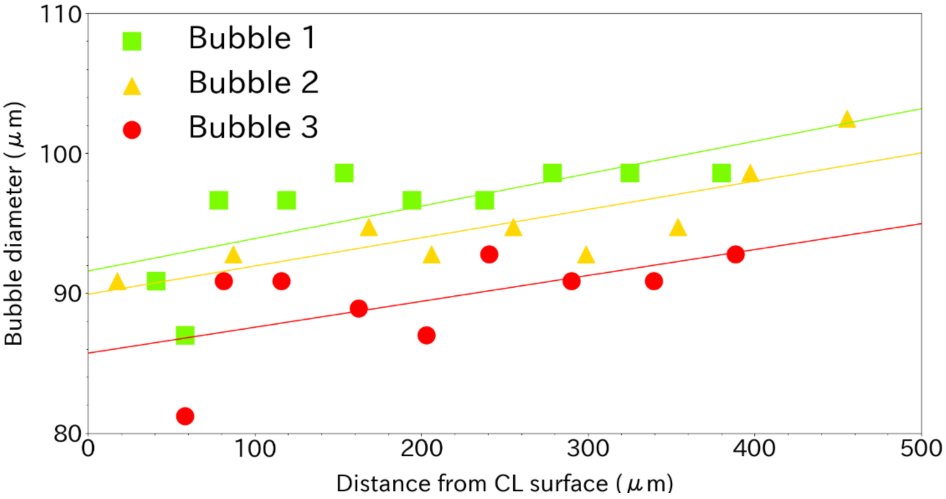

Fig.2 Growth of ascending bubbles during electrolysis at 100 mA cm$^{-2}$ without water flow. The solid lines are linear regression lines obtained using the least-squares method.

### 3-2. Growth rate of static bubbles

The behavior of bubbles near the anode catalyst electrode of PEMWE was observed using a high-speed camera to measure bubble growth. The radius of the bubbles was observed to increase after they detached from the anode CL surface. This bubble growth indicates the presence of dissolved oxygen and oxygen supersaturation regions near the anode CL, and the oxygen produced may be transported not only by bubble migration but also by diffusion of dissolved oxygen. The presence of dissolved oxygen may have certain implications for the design of the porous structure of the anode CL and PTL to reduce anode mass transport losses.

In this experiment, the concentration distribution of dissolved oxygen was examined by investigating the relationship between the volume change of stationary bubbles attached to the wall and their distance from the anode CL surface. Figure 5 shows the relationship between the growth rate of stationary bubbles attached to the wall and the distance from the anode CL surface. The voltage was applied at a constant voltage of 1.5 V, and the current was approximately 0.2 mA. Assuming that the reaction zone is 20 μm wide and 1 cm long, the current density is about 100 mA/cm$^2$ .

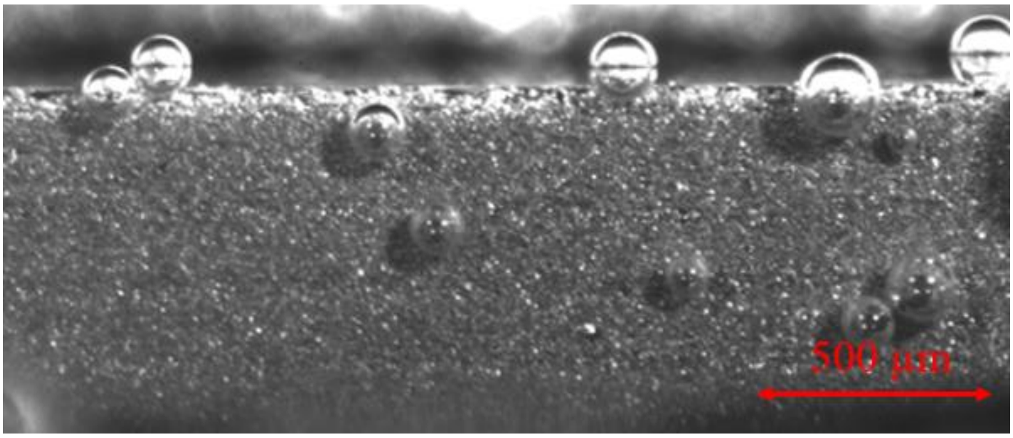

Fig.3 Appearance of shooting when using a glass plate with gold sputtering

As can be seen in Fig.4, the bubble growth rate decreased with increasing distance from the anode CL surface. Therefore, the concentration distribution of dissolved oxygen is expected to decrease with increasing distance from the anode CL surface.

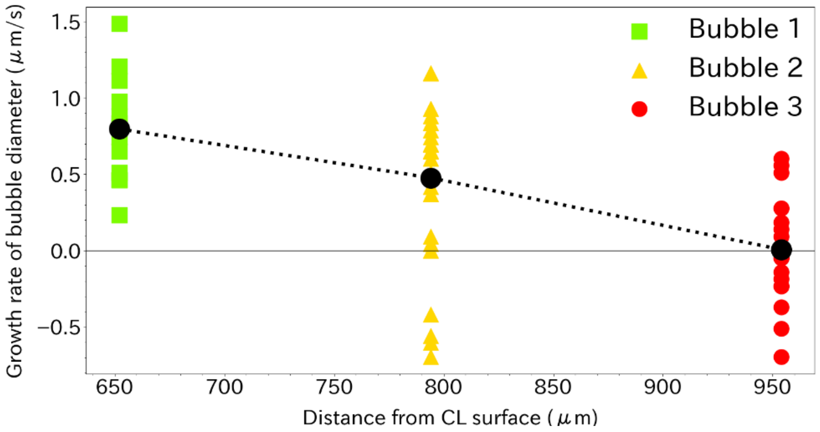

Fig.4 Relationship between bubble growth rate and distance from CL surface

## REFERENCES

[1] Konosuke Watanabe et al, “Existence of Dissolved Oxygen near Anode Catalyst in Proton Exchange Membrane Water Electrolyzers” Journal of The Electrochemical Society, Vol 169, No. 4, (2022), pp. 044515

P23

# CARBON-SUPPORTED SILVER/MANGANESE OXYDE CATALYSTS FOR THE OXYGEN REDUCTION REACTION IN ALKALINE MEDIA

WOLF Sigrid[1], ROSCHGER Michaela[1] and HACKER Viktor[1]

[1]TU Graz, Institute of Chemical Engineering and Environmental Technology, Inffeldgasse 25/C, 8010 Graz, Austria, Sigrid.Wolf@TUGraz.at, Viktor.Hacker@TUGraz.at

**Keywords:** Oxygen reduction reaction, cathode catalysts, alkaline electrolyte, rotating disk electrode analysis.

## INTRODUCTION

Oxygen reduction reaction (ORR) is a complex mechanism that proceeds in two different pathways: direct four-electron reduction (equation 1) and the less efficient, indirect two-step process forming hydrogen peroxide (equation 2), which is further converted to hydroxide ions (equation 3). The development of highly efficient cathode catalysts that predominantly follow the direct pathway is of great interest to increase the performance of alkaline fuel cells. In alkaline media, expensive Pt catalysts can be replaced by cheaper alternatives, such as silver and its alloys, transition metal oxides or metal oxide/carbon composites, while at the same time increasing the activity. The combination of silver and manganese oxides ($Mn_xO_y$) has been shown in the literature to be effective, benefiting from the properties of both materials. In addition to the lower price compared to precious metals, Ag and $Mn_xO_y$ exhibit high ORR activity and stability in alkaline electrolytes. The ORR performance of the catalysts depends strongly on different parameters including preparation methods, manganese valence state, surface morphology and crystalline structure. The catalytic activity is not only influenced by the active material, but also by the choice of a suitable carbon support material. The deposition of nanoparticles on carbon leads to a larger active surface area and thus to an increase in activity and, as a result, also to a reduction of costs, since less active material is required in total. The materials must therefore provide outstanding electronic, thermal and mechanical properties along with a large specific surface area [1, 2].

$$O_2 + 2H_2O + 4e^- \rightarrow 4OH^- \qquad E° = 0.404\ V\ vs.\ RHE \qquad (1)$$

$$O_2 + H_2O + 2e^- \rightarrow HO_2^- + OH^- \qquad E° = 0.080\ V\ vs.\ RHE \qquad (2)$$

$$HO_2^- + H_2O + 2e^- \rightarrow 3OH^- \qquad E° = 0.880\ V\ vs.\ RHE \qquad (3)$$

## EXPERIMENTAL

In this study, Ag-$Mn_xO_y$ is deposited on suitable carbon support materials via a facile synthesis method and the activity and stability of the catalysts towards the ORR was investigated. Comprehensive physicochemical characterization of the synthesized catalysts was carried out to analyse the structure, morphology, chemical composition, specific surface area and thermal properties of the materials. Electrochemical ex-situ characterization was performed by means of thin-film rotating disk electrode experiments in a typical three electrode setup. In order to determine the oxidation and reduction processes and the activity towards oxygen reduction reaction, cyclic voltammograms and linear sweep voltammograms were recorded in $N_2$ purged and oxygen saturated 1 M potassium hydroxide solution. The kinetic properties of the catalysts were determined according to Koutecky-Levich and Tafel analysis. To gain information about the tolerance to ethanol, the measurements are repeated in an alkaline ethanol solution (1 M) and chronoamperometry was performed to examine the stability of the catalysts.

## RESULTS

Ag-$Mn_xO_y$ was successfully deposited on different carbon materials. The catalysts showed high activity and stability towards ORR, which, however, strongly depends on the choice of support material. The morphology of the nanoparticles was influenced by the carbon material choice, which affected the electrochemical results (Fig.1). Low onset potentials of 0.9 V vs. RHE and limiting current density values up to -3.01 mA cm$^{-2}$ (Fig. 2) have been examined. The number of transferred electrons was determined to be about 3.5 by Koutecky-Levich. In addition, high tolerance to ethanol and good stability were found.

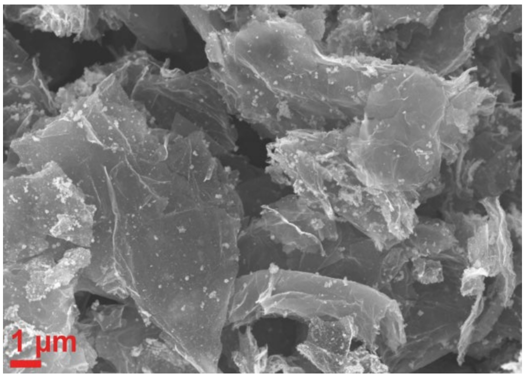

Fig. 1: SEM image of the prepared Ag-Mn$_x$O$_y$/C catalyst [1].

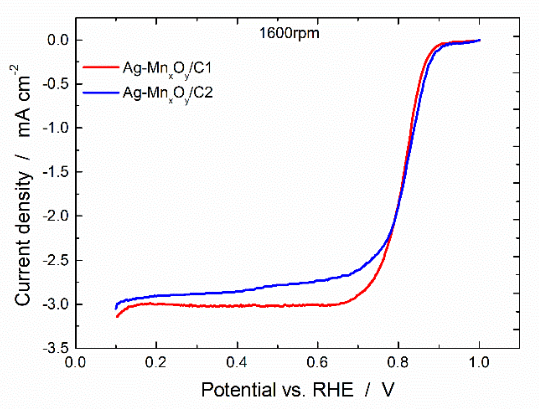

Fig. 2: Linear sweep voltammograms of the synthesized cathode catalysts [1].

ACKNOWLEDGEMENT

The authors acknowledge the financial support by the Austrian Science Fund (FWF): I 3871-N37.

## REFERENCES

[1] S. Wolf, M. Roschger; B. Genorio, M. Kolar, D. Garstenauer, B. Bitschnau and V Hacker, Catalysts 2022, 12, 780

[2] M. Nosan, M. Löffler, I. Jerman, M. Kolar, I. Katsounaros, and B. Genorio, ACS Appl. Energy Mater. 2021

P24

# PREPARATION AND EVALUATION OF HYDROGEL ELECTRODES WITH HIGH RELEASING ABILITY OF EVOLVED BUBBLES

Ritsuki Nakajima,[1] Tatsuya Taniguchi,[2] Yuta Sasaki,[2] Yoshinori Nishiki,[3] Zaenal Awaludin,[3] Takaaki Nakai,[3] Akihiro Kato,[3] Shigenori Mitsushima,[1,4] and Yoshiyuki Kuroda[1,4]
[1]Grad. School of Eng. Sci., Yokohama Natl. Univ., 79-5 Tokiwadai, Hodogaya-ku, Yokohama 240-8501, Japan
[2]Kawasaki Heavy Ind., Ltd., 1-1 Kawasakicho, Akashi, Hyogo, 673-8666, Japan
[3]De Nora Permelec, Ltd., 2023-15 Endo, Fujisawa, Kanagawa, 252-0816, Japan
[4]Adv. Chem. Energy Res. Center, Inst. of Adv. Sci., Yokohama Natl. Univ., 79-5 Tokiwadai, Hodogaya-ku, Yokohama 240-8501, Japan
E-mail: ynugr-cel@ynu.ac.jp

**Keywords:** Alkaline water electrolysis, Hydrogel electrode, Oxygen evolution reaction

## INTRODUCTION

Water electrolysis is a core technology in the conversion of renewable energy to hydrogen. Alkaline water electrolysis (AWE) is one of the most suitable technologies because of its low cost and applicability to large-scale production of hydrogen. To operate AWE at high current density, the use of porous electrodes with a large specific surface area is effective. On the other hand, when the pore size is made smaller in order to increase the surface area, pore blockage due to evolved bubbles should increase. [1] Therefore, in this study, a hydrogel which has a uniform and flexible structure was used for an electrode material to improve the releasing ability of evolved bubbles (Fig. 1).

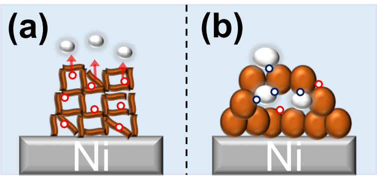

Fig. 1 Illustrations the (a) hydrogel and (b) porous electrodes.

## Experimental

A hybrid cobalt hydroxide nanosheet (Co-ns) was synthesized according to the literature. [2] Electrochemical tests were performed in a 1 M KOH, using a PFA three-electrode cell. A nickel plate, a nickel coil, and a reversible hydrogen electrode (RHE) were used as the working, counter, and reference electrodes, respectively. The Co-ns dispersion (final concentration 40 ppm) was then added in the electrolyte. Co-ns was deposited by chronopotentiometry (CP) at 800 mA cm$^{-2}$ for 0.5 – 50 h (called as the hydrogel electrode, Fig. 2). The catalyst activity was evaluated by cyclic voltammetry (CV) between 0.5 and 1.8 V vs. RHE at 5 mV s$^{-1}$, CV between 0.5 and 1.6 V vs. RHE at 50 mV s$^{-1}$, and electrochemical impedance spectroscopy (EIS) at 1.6 V vs. RHE with the frequency range 0.1–10$^5$ Hz. As a control sample, porous $Co_3O_4$ electrodes (called as the porous electrode) with a rigid framework were prepared by thermal decomposition of $Co(NO_3)_2$. The thickness of catalyst layer was determined by a laser microscope and scanning electron microscope (SEM).

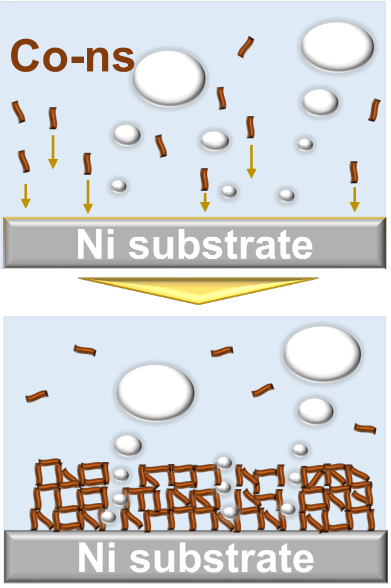

Fig. 2 Illustrations the formation of the catalyst layer by electrolysis

## Results and Discussion

The determined thickness of catalyst layer ($t$) indicated a linear relationship with the amount of catalyst per geometric area; thus, the catalyst layer is uniform along the direction of thickness. The hydrogel electrode exhibited higher OER activity than the porous electrode (Fig. 3). The charge of the anodic peaks due to $Co^{2+/3+}$ and $Co^{3+/4+}$ ($Q_a$), which is in principle proportional to the electrochemically active Co sites, was linearly correlated with $t$. Both samples are assumed to be porous, and the active sites are accessible from electrolyte.

We then define the specific current density ($i^*$) which is a current density at 1.6 V vs. RHE normalized by $Q_a$. When the catalyst layer is thin the specific current density should be hardly affected by the pore blocking due to evolved gas. Thus, we used $i^*/i^*_{max}$ as an indicator of the effect of pore blocking, where $i^*$ is the largest specific current density. Usually, it is considered that the utilization ratio of the reactive sites of porous electrodes decreases as the catalyst layer becomes thicker because of the pore blockages due to evolved bubbles and decreased accessibility of electrolytes. As shown in the Fig. 4, $i^*/i^*_{max}$ of the hydrogel electrode was much higher than those of the porous electrode. The decreased ratio of $i^*/i^*_{max}$ of the hydrogel electrode at $t$ = 15 μm was about 1/5 as large as that of the porous electrode. We propose possible mechanism of this unique property of hydrogel electrodes as (1) the nanopore formed between the nanosheets suppresses the formation of bubbles, (2) high hydrophilicity enhanced the bubble detachment at the electrode interface and (3) the flexible structure of hydrogel contributes to keeping and optimizing the porous structure.

Thus, the potential usefulness of hydrogel electrodes for AWE to suppress the effect of pore blockage was demonstrated. These insights will contribute to achieve the high releasing ability of evolved bubbles for oxygen evolution electrodes.

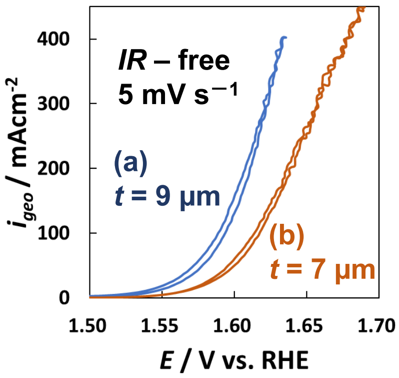

Fig. 3 Polarization curves of the hydrogel and (b) porous electrodes.

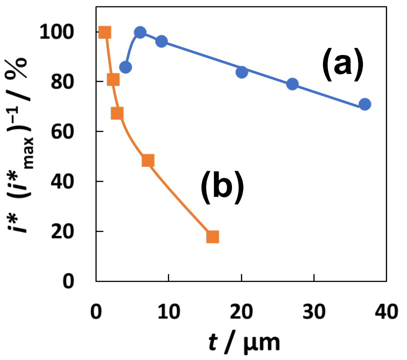

Fig. 4 The change ratio of the OER activity of the (a) hydrogel and (b) porous electrodes as a function of the thickness of catalyst layer.

**Acknowledgements** This work was supported partially by the JSPS KAKENHI from MEXT, Japan.

## REFERENCES

[1] F. Yang *et al.*, *Adv. Energy Mater.*, **10**, 2001174 (2020).
[2] Y. Kuroda *et al.*, *Chem. Eur. J.*, **23**, 5023 (2017).

P25

# VISUALIZATION OF HYDROGEN BUBBLES IN POROUS TRANSPORT LAYER IN TOLUENE DIRECT-ELECTRO-HYDROGNATION ELECTROLYZER USINIG X-RAY-CT SYSTEM

Sunpil Jang[1], Fatima Reyna[2], Kaito Shigemasa[2], Takuto Araki[2],

[1]Department of Mechanical Engineering, Yokohama National University, Kanagawa, Japan, jang-sunpil-gs@ynu.jp
[2] Department of Mechanical Engineering, Yokohama National University, Kanagawa, Japan,

**Keywords:**toluene hydrogenation, methyl cyclo hexane, electrolyzer, hydrogen bubbles, electro chemical.

## INTRODUCTION

Currently, the use of renewable energy is being promoted as an approach to decarbonization. However, renewable energy requires stable energy storage and supply because the amount of electricity is affected by time and climate. One of the solutions is use of hydrogen as an energy source. As the demand for hydrogen increases in the future, a large amount of hydrogen will be needed, and the storage and transportation of large amounts of hydrogen will also be necessary. However, the methods for storing and transporting large amounts of hydrogen have not yet been established, and this is one of the challenges in the current hydrogen utilization. One of the methods for storing and transporting large amounts of hydrogen is the organic hydride method. The organic hydride method is a method of storing and transporting hydrogen using hydrogenation and dehydrogenation of organic compounds. Among these, the use of toluene and methylcyclohexane (MCH) has attracted attention. The advantages of using toluene and MCH include the following: because toluene and MCH are liquids at normal temperature and pressure, they can be transported at about 1/500th the volume of direct hydrogen gas transport; toluene and MCH can be reused; hydrogenation and dehydrogenation are the only reactions, so no byproducts are generated; and they can be transported in the same way as petroleum. Hydrogen can be transported in the same way as petroleum. Therefore, it is expected to be used as a storage and transport medium for hydrogen.

A toluene direct electro hydrogenation electrolyzer is available as a means of hydrogenating toluene. In the toluene direct electro hydrogenation electrolyzer, hydrogen and toluene are supplied to the electrolyzer, and electricity is applied to protonate the hydrogen and supply it to toluene to produce MCH. The advantages are that cost and time losses can be reduced because water electrolysis and toluene hydrogenation can be performed simultaneously, there is no heat loss in the reaction, and the theoretical decomposition voltage can be reduced compared to electrolysis of water and hydrogenation of toluene separately. However, during hydrogenation of toluene, a part of the water being electrolyzed is transferred to the toluene reaction surface, reducing the reaction efficiency to MCH. In addition, part of the protonated hydrogen becomes hydrogen bubbles, which inhibit the fuel supply and reduce the reaction area. Furthermore, the phenomena of water movement and hydrogen bubbles in toluene hydrogenation have not yet been studied.

In this study, we aim to understand the generation of hydrogen bubbles by visualizing the phenomena in toluene hydrogenation using a toluene direct electro hydrogenation electrolyzer with an X-ray CT system, and to provide a guideline for future research on the suppression of hydrogen bubble generation and water movement. Fig. 1 shows a schematic diagram of the toluene direct electro- hydrogenation electrolyzer used in this experiment. The electrolyzer consists of a catalyst layer, a gas diffusion layer (GDL), and a separator, in that order. The electrolyzer is operated by supplying toluene to the anode side and hydrogen to the cathode side, and electricity is supplied. Visualization of the interface between the GDL and catalyst layer on the cathode side of the electrolyzer during operation using an X-ray CT system allows the phenomena on the reaction surface to be visualized. Figure 2 Visualization of the inside of the electrolyzer during operation. Fig. 2 (a) shows the electrolyzer filled with MCH and (b) shows the electrolyzer filled with toluene. The toluene electrolyzer generates fewer hydrogen bubbles, which confirms that the reaction is normal, and the correlation between the current density and the generation of hydrogen bubbles is examined.

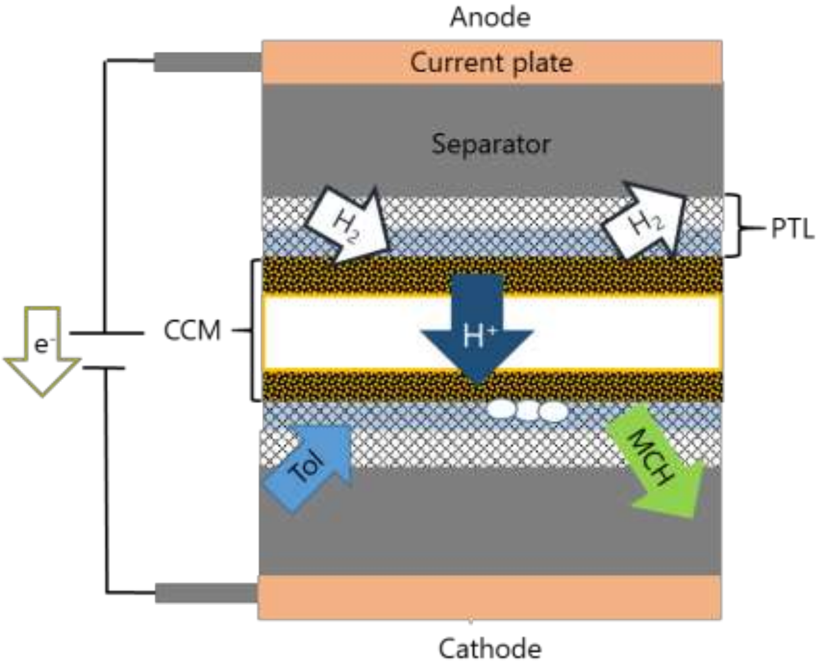

Fig.1 Schematic diagram of toluene direct electro-hydrogenation electrolyze

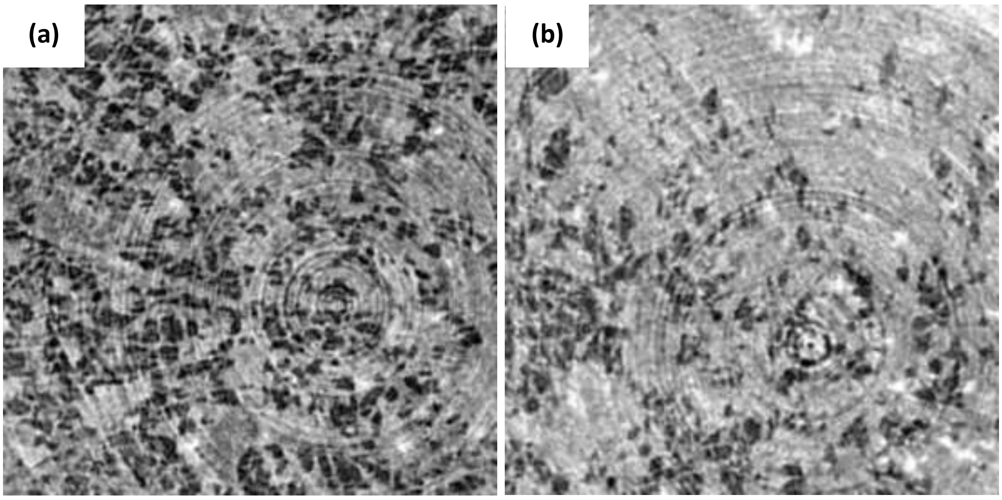

Fig2. Visualization of the inside the electrolyzer during operation

(a) Operate the electrolyzer with MCH (b)Operate the electrolyzer with toluene

## REFERENCES

[1] K. Nagasawa et al., *journal of Power Sources*, 227070-227077, 439 (2019)
[2] K. Nagasawa et al., *Electrochemistry*, 339-344, 86 (2018)
[3] K. Nagasawa et al., *Electrocatalysis*, 164-169, 8 (2017)